IEEE Access
Multidisciplinary | Rapid Review | Open Access Journal

Received 25 July 2023, accepted 16 August 2023, date of publication 24 August 2023, date of current version 6 September 2023.

Digital Object Identifier 10.1109/ACCESS.2023.3308488

RESEARCH ARTICLE

Hybrid Wideband Millimeter Wave Transceiver for Single-User Multi-Relay MIMO Systems

HAFIZ MUHAMMAD TAHIR MUSTAFA[1,2], JUNG-IN BAIK[1,2], YOUNG-HWAN YOU[2,3], ZUNIRA ABBASI[1,2], AND HYOUNG-KYU SONG[1,2]

[1]Department of Information and Communication Engineering, Sejong University, Seoul 05006, Republic of Korea
[2]Department of Convergence Engineering for Intelligent Drone, Sejong University, Seoul 05006, Republic of Korea
[3]Department of Computer Engineering, Sejong University, Seoul 143-747, Republic of Korea

Corresponding author: Hyoung-Kyu Song (songhk@sejong.ac.kr)

This work was supported by the National Research Foundation of Korea (NRF) grant funded by the Korea government (MSIT) (No. NRF-2021R1A2C2005777). This research was supported by Basic Science Research Program through the National Research Foundation of Korea (NRF) funded by the Ministry of Education (2020R1A6A1A03038540). This work was supported by the Technology Innovation Program (RS-2022-00154678, Development of Intelligent Sensor Platform Technology for Connected Sensor) funded By the Ministry of Trade, Industry & Energy (MOTIE, Korea).

ABSTRACT This paper proposes a hybrid wideband millimeter-wave (mm-Wave) beamforming technique for achievable rate maximization in single-user, multi-relay, multi-input multi-output (MIMO) systems. The underlying network architecture is of great practical importance from the perspective of hybrid precoding for enhancing coverage area, transmission range, link quality, and spectral efficiency. In hybrid transceivers, the analog processing component in the radio frequency (RF) section of the system essentially needs to follow an element-wise constant amplitude constraint, which makes the optimization problem non-convex and hence mathematically intractable. Therefore, it is quite a challenging task to obtain the global optimal solution. Moreover, the common analog precoder and combiner are required for different frequency-selective channels in broadband systems, which adds another layer of design complexity. To address this problem, the proposed algorithm transforms the original complicated optimization problem into a relatively simple form. Leveraging this, the complexity of the optimization problem is reduced through decoupled design using the norm preservation property of the unitary transform. Moreover, the analog beamforming design is decomposed into two sub-problems by exploiting statistical independence among the first hop and second hop channels. Each sub-problem is solved to harvest the array gain through RF precoding and combining using an alternative optimization framework. Finally, the frequency-selective baseband processing components are obtained by minimizing interference among transmitted data streams. The spectral efficiency of the proposed scheme is evaluated by changing system parameters under imperfect channel and phase noise (PN). Simulation results demonstrate that the achieved performance is close to full-complexity precoding and outperforms traditional algorithms.

INDEX TERMS Amplify-and-forward relaying, hybrid beamforming, millimeter wave, MIMO, multi-relay.

I. INTRODUCTION

The advanced wireless networks (e.g., fifth generation (5G) and beyond (B5G)) will support several new technologies and services, such as autonomous vehicles, smart environments, remote healthcare, industrial and agricultural automation, and virtual/augmented reality [1]. These modern technologies and services essentially require higher data rates, lower latency, and increased connectivity [2], [3], [4], [5]. To address these challenges, network operators will have to move to mm-Wave and terahertz (THz) frequencies, as these frequency spectrums contain huge bandwidth to meet the ever-increasing demand for network capacity, data rates, and service quality [6], [7]. However, the signal strength decreases rapidly

The associate editor coordinating the review of this manuscript and approving it for publication was Jjun Cheng.

at such high frequencies due to excessive path-loss, rain fading, atmospheric absorption by different gases, and penetration loss. To overcome these unfavorable propagation effects, mm-Wave and THz communication employ a large number of antennas to achieve high beamforming gain and increased signal directivity [8], [9]. Owing to the small wavelength at mm-Wave/THz frequencies, it becomes possible to deploy a large number of antennas packed closely together in a small physical region. It is worth highlighting that the huge propagation loss at mm-Wave/THz frequencies and the blockage sensitivity of transmitted signals at these frequencies make non-line-of-sight (NLOS) communication a major challenge [10]. In this scenario, the cooperative communication paradigm comes into play, which enables efficient transmission of signals from the source to the destination. Moreover, relay-assisted MIMO communication enhances network coverage, link quality, and spectral efficiency [11], [12]. In addition, the deployment and operational costs of a relay node are significantly lower when compared with a base station (BS). There are two main signal processing strategies at relay nodes, known as regenerative and non-regenerative operations. The regenerative schemes perform decoding and encoding of the received signal at each intermediate hop before transmitting to the next hop. On the other hand, non-regenerative schemes forward the received signal to the next station after amplification [13]. Usually, non-regenerative relaying protocol is considered for design simplicity without loss of generality. Furthermore, low-complexity and high security are essential characteristics of non-regenerative relaying techniques.

It is worthwhile to mention that fully digital beamforming is impractical for large-scale MIMO systems as it requires one dedicated RF chain per antenna in an array. Furthermore, the RF chain is quite expensive and power hungry as well, and hence, fully digital precoding in mm-Wave MIMO systems increases hardware complexity, cost, and power consumption [14], [15]. On the other hand, pure analog beamforming provides a cost-effective and power-efficient solution due to the support of only one RF chain. But it causes a considerably low performance that is not favorable in actual practice [16], [17]. Therefore, the notion of hybrid precoding was introduced to achieve a good trade-off between performance and complexity. Hybrid beamforming is realized by decomposing a process into a low-dimensional digital baseband processing component to achieve multiplexing gain and a high-dimensional analog RF processing component to obtain beamforming gain [18]. Note that there is no restriction on the baseband processing matrix except a power constraint, but the RF processing matrix needs to follow an element-wise constant modulus constraint. Simple analog phase-shifters can be used for the practical implementation of phase-only processors.

Normally, two types of hybrid beamforming architectures are used: (1) a fully connected architecture, where each RF chain is connected to all antennas in an array; this structure can achieve performance close to its fully digital counterpart but with a relatively high-power consumption and increased hardware complexity; and (2) a partially connected structure, where each RF chain is connected to a fixed, non-overlapping subset of the antennas. This structure provides energy-efficient hybrid beamforming with relatively low hardware complexity, but at the cost of a small degradation in performance [19], [20], [21]. It is worth noting that partially connected hybrid precoding may not always achieve satisfactory performance [22], [23] for the following reasons: (1) This structure can lead to less accurate beamforming as it is difficult to sustain fine control over the beam (2) A significant degradation in performance may result as the underlying architecture limits the flexibility of large antenna arrays.

A. RELATED WORK

Several hybrid precoding algorithms have been proposed for point-to-point [24], [25], [26], [27] and point-to-multipoint systems [28], [29]. In [24], the authors exploited the sparsity of mm-Wave channels for designing a hybrid beamforming solution using orthogonal matching pursuit (OMP) method. Orthogonal frequency division multiplexing (OFDM)-based hybrid precoding for large-scale MIMO systems was introduced in [25], and the authors of [26] presented a hybrid beamforming design for mm-Wave MIMO systems under wideband assumption by exploiting Alternating Minimization (Alt-Min) algorithms. The authors of [27] developed an efficient hierarchical codebook design strategy for mm-Wave channel estimation with a hybrid precoding architecture. In [28], the authors proposed a joint hybrid precoding design based on manifold optimization to increase the performance of heuristic techniques considering antenna selection for massive MIMO systems. The authors of [29] designed a codebook-based hybrid precoding for mm-Wave multi-user MIMO systems by taking into account the hardware constraints. In [30], partially connected coordinated beamforming training was introduced for mm-Wave and sub-THz systems.

In [31], the authors tried to extend the OMP-based hybrid transceiver algorithm proposed in [24] for single-user relay-assisted MIMO communication networks using the amplify-and-forward (AF) relaying protocol. Moreover, the OMP-based technique given in [24] was further extended to a relay-assisted multi-user MIMO system [32]. The authors of [33] proposed a hybrid precoding design for both the partially connected and fully connected structures, but this technique is restricted to a single-user case. In [34] and [35], an attempt was made to modify the hybrid beamforming algorithm in [24] for hybrid transceiver design in multi-relay MIMO systems. Specifically, the authors of [34] designed hybrid precoder and combiner at the source and destination, respectively, while analog processors were considered at relay stations. Contrary to the previous design, hybrid beamformers were taken into account at all communicating nodes in [35]. The authors of [36] used codebooks to drive the RF and

baseband processing components separately in a single-relay multi-user system, and this technique was adopted to avoid an intractable searching problem. In [37], the authors addressed a matrix factorization problem for hybrid transceiver design considering the alternating direction method of multipliers (ADMM), and this technique did not require any codebook for the selection of beamforming vectors.

In [38], the authors proposed low-complexity hybrid precoding and diversity combining by exploiting the angular-domain sparsity of the mm-Wave channel. The authors of [39] suggested non-uniform quantization codebook-based hybrid beamforming algorithms for fully connected and partially connected architectures to reduce the feedback overhead. In [40], hybrid wideband mm-Wave transmit precoding was designed by exploiting the channel's covariance matrix and the angle of departure information for multi-user MIMO systems. Furthermore, the effect of beam squint was also minimized using the phase compensation mechanism. In [41], the authors developed hybrid wideband mm-Wave transmit precoding techniques for constructing analog beamformer common to all sub-carriers, considering the effect of beam squint.

B. MOTIVATION

The fundamental concern in this work is to design a hybrid wideband mm-Wave transceiver for a multi-relay MIMO system, as practical broadband systems are frequency-selective in nature. Furthermore, the underlying network architecture can increase transmission range, network coverage area, and achievable rate. Therefore, these networks are of great practical significance when hybrid structures are considered at all communicating nodes. The hybrid processing matrices need to be derived considering channel estimation error and PN to make the design robust. To achieve this target, the proposed algorithm uses tensor decomposition on the first-hop and second-hop channels to derive the common analog RF precoder and combiner at the source and destination, respectively. Then, the iterative procedure based on L_1-norm maximization is followed to design the RF beamforming solution at relay nodes. Finally, digital baseband processing components at various communicating nodes, corresponding to different sub-carriers, are derived by indirectly minimizing inference among transmitted data streams.

C. CONTRIBUTION

The contribution of the proposed scheme can be summarized as follows:

- A novel hybrid wideband transceiver design is proposed for multi-relay MIMO systems for achievable rate maximization, where an attempt is made to exploit the property of unitary transform to decouple the design of analog RF and digital baseband processing components. Then, the complicated optimization problem is decomposed into sub-problems using the notion of statistical independence between the first hop and second hop channels. Furthermore, each sub-problem is tackled using an alternating optimization approach for deriving the RF beamforming solution at relay nodes. Finally, the digital baseband processing components are obtained by minimizing interference among different sub-channels in the equivalent baseband channel corresponding to different sub-carriers.
- To achieve good performance in the presence of channel estimation error and acceptable performance considering PN in hybrid processing matrices, the optimization problem is transformed into L_1-norm maximization problem, which is a robust technique when outliers in the form of channel error and PN exist in the underlying data.
- Computer simulations are conducted by changing system parameters to evaluate the performance of the proposed hybrid precoding for broadband systems, considering channel estimation error with different accuracy factors such as 90%, 80%, and 70%. The obtained results reveal that the presented technique shows good performance when compared with full-complexity precoding. Moreover, the performance degradation occurs in a gradual fashion by increasing the channel estimation error.
- The impact of PN on the performance of the proposed hybrid beamforming scheme is also observed in the simulation results. It is evident from the obtained results that performance degradation occurs when PN is included in hybrid processing components. In addition, the performance achieved by contributing PN is approximately equal to the performance attained with a 20% channel estimation error.

The rest of this paper is organized as follows. System model and problem formulation are given in Section II. Analog RF beamforming solution, at different communicating nodes, is illustrated in Section III. Digital baseband processing components corresponding to different sub-carriers are derived in Section IV. Computational complexity of the proposed algorithm is provided in Section V. Computer simulations for the performance evaluation are included in Section VI. Concluding remarks are given in Section VII.

Notation: Upper-case and lower-case letters $\boldsymbol{A}$ and $\boldsymbol{a}$ denote a matrix and vector, respectively. For a given matrix $\boldsymbol{A}$; $\|\boldsymbol{A}\|_F$, $\|\boldsymbol{A}\|_1$, $\boldsymbol{A}(:, i)$, $\boldsymbol{A}(:, 1:j)$, $Tr(\boldsymbol{A})$, $\det(\boldsymbol{A})$, $\boldsymbol{A}^T$, $\boldsymbol{A}^H$, $\angle\boldsymbol{A}$ and $|\boldsymbol{A}(i, j)|$ denote the Frobenius norm, L_1-norm, i^{th} column, first j columns, trace, determinant, transpose, conjugate transpose, element-wise phase, and the element-wise modulus of a matrix $\boldsymbol{A}$, respectively. $\mathbb{C}$ denotes the field of complex numbers and $\boldsymbol{I}_m$ is the $m \times m$ identity matrix, and $\mathcal{CN}\left(\boldsymbol{0},\ \sigma^2\boldsymbol{I}_n\right)$ is the complex Gaussian distribution with mean $\boldsymbol{0}$ and covariance matrix $\sigma^2\boldsymbol{I}_n$. $\sqcup_r$, $\times_r$ $(r = 1, 2, 3)$ represent the concatenation of tensors or matrices along the r^{th} dimension [42] and $r-$mode product between a tensor and matrix [43], respectively. $bd(\boldsymbol{A}_1, \ldots, \boldsymbol{A}_K)$ shows a block diagonal matrix with sub-matrices $\boldsymbol{A}_1, \ldots, \boldsymbol{A}_K$, $diag(a_1, \ldots, a_K)$ specifies diagonal matrix, and $\mathbb{E}[.]$ denotes the expectation of the argument.

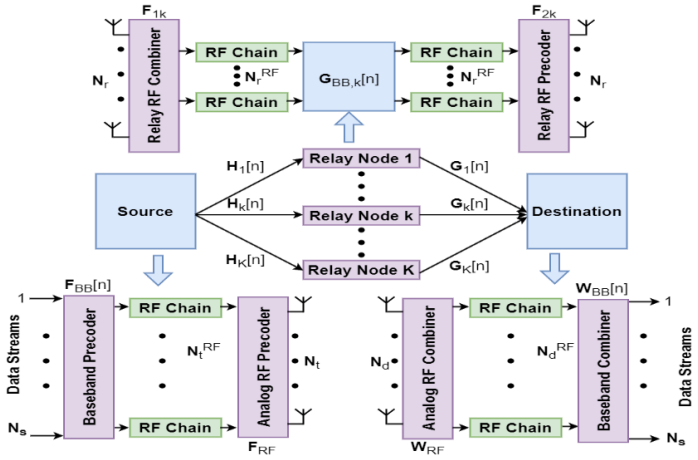

FIGURE 1. Block diagram of the proposed hybrid transceiver for a single-user multi-relay MIMO system.

II. SYSTEM MODEL AND PROBLEM FORMULATION

A. SYSTEM MODEL

Fig. 1 shows the system model of a single-user multi-relay MIMO system, where multiple antennas are deployed at each communicating node. All relay nodes are operating in half-duplex mode using AF relaying protocol. Furthermore, it is assumed that the direct transmission link between the source and destination is not favorable due to excessive path-loss and deep fading. The number of antennas at the source, each relay node, and destination are denoted as N_t, N_r and N_d, and the number of RF chains is specified by N_t^{RF}, N_r^{RF} and N_d^{RF}, respectively. There are N_{sub} sub-carriers for the transmission of data streams. Let $\boldsymbol{s}[n] = \{s_1[n], s_2[n], \ldots, s_{N_s}[n]\} \in \mathbb{C}^{N_s \times 1}$, $n \in \{1, .., N_{sub}\}$ be a complex information symbol vector consisting of N_s data- streams such that $\mathbb{E}\{\boldsymbol{s}[n]\boldsymbol{s}[n]^H\} = \boldsymbol{I}_{N_s}$. Note that the system must satisfy the condition $N_s \leq min\left(N_t^{RF}, N_r^{RF}, N_d^{RF}\right) \ll min\left(N_t, N_r, N_d\right)$ to ensure effective multi-stream transmission.

After hybrid precoding, the transmitted signal from the source $\boldsymbol{x}_s[n] \in \mathbb{C}^{N_t \times 1}$ on the n^{th} frequency-carrier can be expressed as

$$\boldsymbol{x}_s[n] = \boldsymbol{F}_{RF}\boldsymbol{F}_{BB}[n]\boldsymbol{s}[n], \tag{1}$$

where $\boldsymbol{F}_{RF} \in \mathbb{C}^{N_t \times N_t^{RF}}$ and $\boldsymbol{F}_{BB}[n] \in \mathbb{C}^{N_t^{RF} \times N_s}$ are the analog beamformer common to all sub-carriers and the digital baseband processing component corresponding to the n^{th} frequency-carrier at the source, respectively. The transmit power constraint at the source is given as

$$\|\boldsymbol{F}_{RF}\boldsymbol{F}_{BB}[n]\|_F^2 \leq N_s, \ \forall n \in \{1, \ldots, N_{sub}\}. \tag{2}$$

In relay-assisted networks, two time slots are required for the transmission of signal from the source to the destination. In the first time slot, each relay station receives the source transmitted signal, and the processed signal is transmitted to the destination in the second time slot. This functionality at the relay node essentially requires a hybrid combiner to process the received signal and a hybrid precoder to transmit the processed signal to the destination. Let $\boldsymbol{F}_{1k} \in \mathbb{C}^{N_r \times N_r^{RF}}$ be the RF combiner and $\boldsymbol{F}_{2k} \in \mathbb{C}^{N_r \times N_r^{RF}}$ be the RF precoder at the k^{th} relay node, which are common to all sub-carriers. The corresponding baseband combiner and precoder at the n^{th} frequency-carrier are represented by $\boldsymbol{G}_{BB1,k}[n] \in \mathbb{C}^{N_r^{RF} \times N_s}$ and $\boldsymbol{G}_{BB2,k}[n] \in \mathbb{C}^{N_r^{RF} \times N_s}$, respectively. The hybrid relay filter $\boldsymbol{F}_k[n] \in \mathbb{C}^{N_r \times N_r}$ at the k^{th} relay station corresponding to the n^{th} sub-carrier, using $\boldsymbol{F}_{1k}$, $\boldsymbol{F}_{2k}$, $\boldsymbol{G}_{BB1,k}[n]$ and $\boldsymbol{G}_{BB2,k}[n]$, can be expressed as

$$\begin{aligned}\boldsymbol{F}_k[n] &= \boldsymbol{F}_{2k}\boldsymbol{G}_{BB2,k}[n]\boldsymbol{G}_{BB1,k}^H[n]\boldsymbol{F}_{1k}^H \\ &= \boldsymbol{F}_{2k}\boldsymbol{G}_{BB,k}[n]\boldsymbol{F}_{1k}^H,\end{aligned} \tag{3}$$

where $\boldsymbol{G}_{BB,k}[n] = \boldsymbol{G}_{BB2,k}[n]\boldsymbol{G}_{BB1,k}^H[n] \in \mathbb{C}^{N_r^{RF} \times N_r^{RF}}$ is the combined baseband processing matrix at the k^{th} relay station. The received signal at the k^{th} relay node $\boldsymbol{y}_k[n] \in \mathbb{C}^{N_r \times 1}$ can be written as

$$\boldsymbol{y}_k[n] = \boldsymbol{H}_k[n]\boldsymbol{F}_{RF}\boldsymbol{F}_{BB}[n]\boldsymbol{s}[n] + \boldsymbol{n}_k[n], \tag{4}$$

where $\boldsymbol{H}_k[n] \in \mathbb{C}^{N_r \times N_t}$ and $\boldsymbol{n}_k[n] \in \mathbb{C}^{N_r \times 1}$ are the channel matrix between the source and the k^{th} relay node, and zero mean circularly symmetric complex Gaussian (ZMCSCG) noise with variance σ_k^2, i.e., $\boldsymbol{n}_k[n]$ $\mathcal{CN}\left(0, \sigma_k^2\boldsymbol{I}_{N_r}\right)$, respectively. When $\boldsymbol{y}_k[n]$ (4) is passed through the relay filter $\boldsymbol{F}_k[n]$ (3) then the transmitted signal from the k^{th} relay node can be characterized as

$$\begin{aligned}\boldsymbol{x}_k[n] &= \boldsymbol{F}_k[n]\boldsymbol{y}_k[n] \\ &= \boldsymbol{F}_{2k}\boldsymbol{G}_{BB,k}[n]\boldsymbol{F}_{1k}^H\left(\boldsymbol{H}_k[n]\boldsymbol{F}_{RF}\boldsymbol{F}_{BB}[n]\boldsymbol{s}[n] + \boldsymbol{n}_k[n]\right).\end{aligned} \tag{5}$$

The transmit power at the k^{th} relay station, using (5), is given as

$$Tr\left\{\boldsymbol{F}_k[n]\left((\boldsymbol{H}_k[n]\boldsymbol{F}_{RF}\boldsymbol{F}_{BB}[n])(\boldsymbol{H}_k[n]\boldsymbol{F}_{RF}\boldsymbol{F}_{BB}[n])^H + \sigma_r^2\boldsymbol{I}_{N_r}\right)\boldsymbol{F}_k^H[n]\right\} \leq P_{r,k},\ \forall, k, n. \tag{6}$$

Using (5), the received signal at the destination $\boldsymbol{y}_d[n] \in \mathbb{C}^{N_d \times 1}$ through K relay nodes can be expressed as

$$\begin{aligned}\boldsymbol{y}_d[n] &= \sum_{k=1}^{K}\boldsymbol{G}_k[n]\boldsymbol{x}_k[n] + \boldsymbol{z}[n] \\ &= \sum_{k=1}^{K}\boldsymbol{G}_k[n]\boldsymbol{F}_k[n](\boldsymbol{H}_k[n]\boldsymbol{F}_{RF}\boldsymbol{F}_{BB}[n]\boldsymbol{s}[n] + \boldsymbol{n}_k[n]) \\ &\quad + \boldsymbol{z}[n],\end{aligned} \tag{7}$$

where $\boldsymbol{G}_k[n] \in \mathbb{C}^{N_d \times N_r}$ and $\boldsymbol{z}[n] \in \mathbb{C}^{N_d \times 1}$ are the channel matrix between the k^{th} relay node and destination, and ZMCSCG noise with variance σ_d^2 i.e., $\boldsymbol{z}[n]\ \mathcal{CN}\left(0,\ \sigma_d^2\boldsymbol{I}_{N_d}\right)$, respectively. Finally, the received signal at the destination $\boldsymbol{y}[n] \in \mathbb{C}^{N_s \times 1}$ after applying hybrid combiner is given as (8), shown at the bottom of the next page, where $\boldsymbol{W}_{RF} \in \mathbb{C}^{N_d \times N_d^{RF}}$ and $\boldsymbol{W}_{BB}[n] \in \mathbb{C}^{N_d^{RF} \times N_s}$ are the common analog RF combiner and digital baseband processing component corresponding to the n^{th} frequency sub-carrier at the destination, respectively. Moreover, $\boldsymbol{H}[n] = \left[\boldsymbol{H}_1^T[n], \ldots, \boldsymbol{H}_K^T[n]\right]^T \in \mathbb{C}^{KN_r \times N_t}$, $\boldsymbol{G}[n] = [\boldsymbol{G}_1[n], \ldots, \boldsymbol{G}_K[n]] \in \mathbb{C}^{N_d \times KN_r}$, $\boldsymbol{n}[n] = \left[\boldsymbol{n}_1^T[n], \ldots, \boldsymbol{n}_K^T[n]\right]^T \in \mathbb{C}^{KN_r \times 1}$ and $\boldsymbol{F}[n] = bd\left(\boldsymbol{F}_1[n], \ldots, \boldsymbol{F}_K[n]\right) \in \mathbb{C}^{KN_r \times KN_r}$ denote the first-hop channel, second-hop channel, combined noise vector of K relay nodes with $\boldsymbol{n}[n]\ \mathcal{CN}\left(0,\ \sigma_r^2\boldsymbol{I}_{KN_r}\right)$, and block diagonal matrix of hybrid relay filterers due to the spatial distribution of relay stations, respectively. The compact representation of (8) is given as

$$\boldsymbol{y}_F[n] = \boldsymbol{A}[n]\boldsymbol{s}[n] + \boldsymbol{v}[n], \tag{9}$$

where

$$\begin{cases}\boldsymbol{A}[n] \triangleq (\boldsymbol{W}_{RF}\boldsymbol{W}_{BB}[n])^H\boldsymbol{G}[n]\boldsymbol{F}[n]\boldsymbol{H}[n]\boldsymbol{F}_{RF}\boldsymbol{F}_{BB}[n] \\ \boldsymbol{v}[n] \triangleq (\boldsymbol{W}_{RF}\boldsymbol{W}_{BB}[n])^H\boldsymbol{G}[n]\boldsymbol{F}[n]\boldsymbol{n}[n] \\ +(\boldsymbol{W}_{RF}\boldsymbol{W}_{BB}[n])^H\boldsymbol{z}[n]\end{cases}$$

Using (9), the achievable rate averaged over N_{sub} sub-carriers can be obtained as

$$R = \left(\frac{1}{N_{sub}}\right)\sum_{n=1}^{N_{sub}}\left(\frac{1}{2}\right)log_2 det\left(\boldsymbol{I}_{N_s} + \boldsymbol{A}[n]\boldsymbol{R}_N^{-1}[n]\boldsymbol{A}^H[n]\right) \times \left(\frac{bps}{Hz}\right), \tag{10}$$

where

$$\begin{aligned}\boldsymbol{R}_N &= \mathbb{E}\left[\boldsymbol{v}[n]\boldsymbol{v}^H[n]\right] \\ &= \sigma_r^2\{(\boldsymbol{W}_{RF}\boldsymbol{W}_{BB}[n])^H\boldsymbol{G}[n]\boldsymbol{F}[n]\} \\ &\quad \times \left\{(\boldsymbol{W}_{RF}\boldsymbol{W}_{BB}[n])^H\boldsymbol{G}[n]\boldsymbol{F}[n]\right\}^H \\ &\quad + \sigma_d^2(\boldsymbol{W}_{RF}\boldsymbol{W}_{BB}[n])^H(\boldsymbol{W}_{RF}\boldsymbol{W}_{BB}[n])\end{aligned}$$

is the equivalent noise covariance matrix. The scaling factor (1/2) in (10) shows that the achievable rate reduces by one-half as data transmission from the source to the destination takes two time-instances.

B. PROBLEM FORMULATION

In this work, the main objective is to maximize the achievable rate in (10) by deriving a hybrid beamforming solution at different communicating nodes of the underlying system when frequency-selective fading comes into play. To achieve this target, the optimization problem is formulated in (11), as shown at the bottom of the next page, where R is defined in (10). The coupling between the analog and digital beamforming components, and the element-wise constant amplitude constraint imposed by the RF processing matrices make the problem (11) non-convex, non-linear, and often intractable [44]. Therefore, an attempt to directly solve this problem is mathematically challenging that requires joint optimization of RF and baseband processing components to achieve global optimal performance. Note that fully digital precoding for multi-relay MIMO systems is also quite complicated, and an alternating optimization framework is usually employed to approach the optimal solution. In the context of hybrid beamforming, a decoupled approach is normally followed, where the RF and baseband processing components are designed separately to facilitate a low-complexity solution. It is possible to transform the original complicated optimization problem (11) into a relatively simple form that can also lead to the same end goal. (Proof: Appendix A) Therefore, the reformulated problem is given in (12), as shown at the bottom of the next page, where $\boldsymbol{A}[n] \triangleq (\boldsymbol{W}_{RF}\boldsymbol{W}_{BB}[n])^H\boldsymbol{G}[n]\boldsymbol{F}[n]\boldsymbol{H}[n]\boldsymbol{F}_{RF}\boldsymbol{F}_{BB}[n]$.

The objective function in (12) corresponds to the received power at the destination, i.e., $\boldsymbol{Tr}\{\boldsymbol{A}[n]\boldsymbol{A}^H[n]\} = \|\boldsymbol{A}[n]\|_F^2$ (9), and hence, this approximation of the original objective function is considered to be a valid, and the achievable rate maximization can also be obtained by solving the reformulated problem as mentioned in (12). While solving this problem, an attempt is made to decouple the analog RF and digital baseband processing components. This task can be achieved by assuming that the analog beamforming solution is known at different communicating nodes. In this case, the objective function $Tr\{\boldsymbol{A}[n]\boldsymbol{A}^H[n]\}$ can be maximized considering that the baseband processing components are unitary matrices. The condition associated with baseband processing matrices lead to the function $Tr\{\boldsymbol{A}[n]\boldsymbol{A}^H[n]\}$ that contains the RF beamforming matrices only. After decoupling the baseband processing components under unitary transform, the resultant function consisting of phase-only processing components can be decomposed into two factors by exploiting the statistical independence property. This process facilitates converting the optimization problem (12) into two independent sub-problems. These sub-problems are transformed into L_1-norm maximization problems, as it is required to find the analog RF processing

components that maximize the achievable rate in the presence of channel estimation error and phase noise in hybrid beamformer. Finally, the required digital baseband processing components are derived by diagonalizing the corresponding equivalent baseband channels. In summary, the solution of optimization problem demands to find the list of decision variables $\left(\boldsymbol{F}_{RF},\ \boldsymbol{F}_{BB}[n],\ \boldsymbol{F}_{2k},\ \boldsymbol{G}_{BB2,k}[n],\boldsymbol{G}_{BB1,k}[n],\ \boldsymbol{F}_{1k},\ \boldsymbol{W}_{RF},\boldsymbol{W}_{BB}[n]\right)$ that lead to the achievable rate maximization.

C. IMPERFECT CHANNEL FOR ROBUST DESIGN

It is hard to acquire perfect CSI in actual practice, as there always exists an estimation/quantization error while obtaining the channel matrix. Therefore, imperfect CSI needs to be considered for the robust design of RF and baseband processing components at different communicating nodes. The conventional channel estimation algorithms are not feasible for large-scale mm-Wave MIMO systems owing to the large training overhead. To circumvent this problem, recent CSI estimation techniques exploit the angular-domain sparsity of massive MIMO systems, and compressed sensing (CS) tools can be employed to resolve the problem with reduced training overhead. Furthermore, the mm-Wave channel estimation problem is transformed into estimating the parameters of dominant propagation paths, for instance, complex path gains, angles-of-arrival, and angles-of-departure. In addition, deep learning (DL) models are quite effective in acquiring CSI with minimum estimation error, and more importantly, these DL algorithms shift the computational burden from real-time to the off-line training process. Note that the novel wideband mm-Wave channel estimation algorithm is beyond the scope of this paper, and hence, this topic is left for future work. To make the proposed hybrid transceiver design robust, imperfect channels are considered in the optimization problem (12) for deriving the analog RF and digital baseband processing components. Without loss of generality, the estimated channels $\boldsymbol{G}_k[n]$ and $\boldsymbol{H}_k[n]$ for design simplicity can be modeled as [45]

$$\boldsymbol{G}_k[n] = \bar{\delta}\overline{\boldsymbol{G}_k}[n] + \sqrt{1-\delta^2}\boldsymbol{E}, \tag{12a}$$

$$\boldsymbol{H}_k[n] = \bar{\delta}\overline{\boldsymbol{H}_k}[n] + \sqrt{1-\delta^2}\boldsymbol{E}, \tag{12b}$$

where $\overline{\boldsymbol{H}_k}[n]$ denotes the perfect channel matrix between the source and the k^{th} relay station, $\overline{\boldsymbol{G}_k}[n]$ represents the ideal channel matrix between the destination and the k^{th} relay node, $\delta \in [0,\ 1]$ indicates the accuracy of the estimated CSI, and $\boldsymbol{E}$ is the error matrix that contains independent and identically distributed $(i.i.d)$ Gaussian random variables, i.e., $\mathcal{CN}(0,\ 1)$.

III. PROPOSED HYBRID BEAMFORMING

A. ANALOG BEAMFORMING AT COMMUNICATING NODES

Before deriving the RF beamforming solution at each communicating node, the reformulated problem (12) is decomposed into two independent sub-problems. As

$$Tr\left\{\boldsymbol{A}[n]\boldsymbol{A}^H[n]\right\} = \left\|\boldsymbol{W}_{BB}^H[n]\boldsymbol{W}_{RF}^H\boldsymbol{G}[n]\boldsymbol{F}[n]\boldsymbol{H}[n]\boldsymbol{F}_{RF}\boldsymbol{F}_{BB}[n]\right\|_F^2. \tag{13}$$

Using the definition of $\boldsymbol{H}[n]$, $\boldsymbol{F}[n]$ and $\boldsymbol{G}[n]$ given in Section II, the relation in (13) can also be written in (14), as shown at the bottom of page 8, where $\boldsymbol{F}_k[n] = \boldsymbol{F}_{2k}\boldsymbol{G}_{BB2,k}[n]\boldsymbol{G}_{BB1,k}^H[n]\boldsymbol{F}_{1k}^H$. It is known that $\|\boldsymbol{A}_1 + \ldots + \boldsymbol{A}_K\|_F^2 \le \|\boldsymbol{A}_1\|_F^2 + \ldots + \|\boldsymbol{A}_K\|_F^2$, and hence, the relation in (14) can be expressed in (15), as shown at the bottom of page 8. Moreover, the inequality $\|\boldsymbol{A}_1\boldsymbol{A}_2\|_F^2 \le \|\boldsymbol{A}_1\|_F^2\|\boldsymbol{A}_2\|_F^2$ transforms the result

$$\begin{aligned}\boldsymbol{y}[n] &= (\boldsymbol{W}_{RF}\boldsymbol{W}_{BB}[n])^H\left\{\sum_{k=1}^{K}\boldsymbol{G}_k[n]\boldsymbol{F}_k[n](\boldsymbol{H}_k[n]\boldsymbol{F}_{RF}\boldsymbol{F}_{BB}[n]\boldsymbol{s}[n] + \boldsymbol{n}_k[n]) + \boldsymbol{z}[n]\right\}\\ &= (\boldsymbol{W}_{RF}\boldsymbol{W}_{BB}[n])^H\boldsymbol{G}[n]\boldsymbol{F}[n]\boldsymbol{H}[n]\boldsymbol{F}_{RF}\boldsymbol{F}_{BB}[n]\boldsymbol{s}[n] + (\boldsymbol{W}_{RF}\boldsymbol{W}_{BB}[n])^H\boldsymbol{G}[n]\boldsymbol{F}[n]\boldsymbol{n}[n] + (\boldsymbol{W}_{RF}\boldsymbol{W}_{BB}[n])^H\boldsymbol{z}[n],\end{aligned} \tag{8}$$

$$\begin{aligned}&\max_{[\boldsymbol{F}_{RF},\boldsymbol{F}_{BB}[n],\ \boldsymbol{F}_{2k},\boldsymbol{G}_{BB2,k}[n],\ \boldsymbol{G}_{BB1,k}[n],\boldsymbol{F}_{1k},\ \boldsymbol{W}_{RF},\boldsymbol{W}_{BB}[n]]} R\\ &s.t.\ \|\boldsymbol{F}_{RF}\boldsymbol{F}_{BB}[n]\|_F^2 \le P_s,\\ &Tr\left\{\boldsymbol{F}_k[n]\left((\boldsymbol{H}_k[n]\boldsymbol{F}_{RF}\boldsymbol{F}_{BB}[n])(\boldsymbol{H}_k[n]\boldsymbol{F}_{RF}\boldsymbol{F}_{BB}[n])^H + \sigma_r^2\boldsymbol{I}_{N_r}\right)\boldsymbol{F}_k^H[n]\right\} \le P_{r,k},\ \forall, k, n,\\ &|\boldsymbol{F}_{RF}(x,y)| = \frac{1}{\sqrt{N_t}},\ |\boldsymbol{F}_{1k}(x,y)| = \frac{1}{\sqrt{N_r}},\ |\boldsymbol{F}_{2k}(x,y)| = \frac{1}{\sqrt{N_r}},\ \ |\boldsymbol{W}_{RF}(x,y)| = \frac{1}{\sqrt{N_d}},\ \forall\, x, y,\end{aligned} \tag{11}$$

$$\begin{aligned}&\max_{[\boldsymbol{F}_{RF},\boldsymbol{F}_{BB}[n],\ \boldsymbol{F}_{2k},\boldsymbol{G}_{BB2,k}[n],\ \boldsymbol{G}_{BB1,k}[n],\boldsymbol{F}_{1k},\ \boldsymbol{W}_{RF},\boldsymbol{W}_{BB}[n]]} Tr\{\boldsymbol{A}[n]\boldsymbol{A}^H[n]\}\\ &s.t.\ \|\boldsymbol{F}_{RF}\boldsymbol{F}_{BB}[n]\|_F^2 \le P_s,\\ &Tr\left\{\boldsymbol{F}_k[n]\left((\boldsymbol{H}_k[n]\boldsymbol{F}_{RF}\boldsymbol{F}_{BB}[n])(\boldsymbol{H}_k[n]\boldsymbol{F}_{RF}\boldsymbol{F}_{BB}[n])^H + \sigma_r^2\boldsymbol{I}_{N_r}\right)\boldsymbol{F}_k^H[n]\right\} \le P_{r,k},\ \forall, k, n,\\ &|\boldsymbol{F}_{RF}(x,y)| = \frac{1}{\sqrt{N_t}},\ |\boldsymbol{F}_{1k}(x,y)| = \frac{1}{\sqrt{N_r}},\ |\boldsymbol{F}_{2k}(x,y)| = \frac{1}{\sqrt{N_r}},\ \ |\boldsymbol{W}_{RF}(x,y)| = \frac{1}{\sqrt{N_d}},\ \forall\, x, y,\end{aligned} \tag{12}$$

obtained in (15) into the following form in (16), as shown at the bottom of the next page. Applying summation on the independent factors individually leads to the following product (17), as shown at the bottom of the next page. Under the assumption of given RF beamforming solution at different communicating nodes (i.e., $\boldsymbol{F}_{RF}$, $\boldsymbol{F}_{1k}$, $\boldsymbol{F}_{2k}$, $\boldsymbol{W}_{RF}$), the optimal baseband processing components can be obtained by minimizing interference among transmitted data streams indirectly through diagonalizing the corresponding baseband equivalent channels [46]. It is obvious from this process that baseband processing components, so obtained, are unitary matrices. Furthermore, the norm of a matrix remains constant under unitary transform. This norm preservation property allows to modify the product in (17) as (18), shown at the bottom of the next page. Now, the objective function in (12) for the achievable rate maximization can be further approximated in (19), as shown at the bottom of the next page. The above result reveals that the achievable rate maximization can be obtained by maximizing the product of the sum of the equivalent baseband channels over K relay nodes in the first-hop and second-hop.

Using (19), the optimization problem in (12) can be converted into a simplified form in (20), as shown at the bottom of the next page. The cost function in (20) contains the product of the sum of first-hop and second-hop baseband equivalent channels over K relay nodes. It is worth mentioning that the source analog beamformer $\boldsymbol{F}_{RF}$ and the destination analog combiner $\boldsymbol{W}_{RF}$ are common to N_{sub} sub-carriers and K relay stations to achieve beamforming gain.

Moreover, these factors are independent of each other. One factor contains the RF beamforming components ($\boldsymbol{F}_{1k}$, $\boldsymbol{F}_{RF}$) corresponding to the first-hop of the network, and the other factor comprises of the analog processing matrices ($\boldsymbol{F}_{2k}$, $\boldsymbol{W}_{RF}$) corresponding to the second-hop of the system. Also, the channels from source-to-relay nodes and relay stations-to-destination are statistically independent.

Under the wideband assumption, it is quite complicated to derive the frequency-independent phase-only processing matrices at different communicating nodes without following the decoupling strategy. To reduce the complexity associated with the joint optimization of problem (20), the property of statistical independence is exploited to decompose it into two sub-problems for deriving the required RF processing components as

$$\begin{aligned}
&[\boldsymbol{F}_{RF},\ \boldsymbol{F}_{1k}],\ \max_{n\in\{1,\ldots,N_{sub}\}} \left(\sum_{k=1}^{K}\left\|\left(\boldsymbol{F}_{1k}^{H}\boldsymbol{H}_k[n]\boldsymbol{F}_{RF}\right)\right\|_F^2\right)\\
&\quad s.t.\ \|\boldsymbol{F}_{RF}\boldsymbol{F}_{BB}[n]\|_F^2 \le P_s,\\
&\quad |\boldsymbol{F}_{RF}(x,y)| = \frac{1}{\sqrt{N_t}},\ |\boldsymbol{F}_{1k}(x,y)|\\
&\quad = \frac{1}{\sqrt{N_r}},\ \forall\, x,y,
\end{aligned} \tag{21}$$

$$\begin{aligned}
&[\boldsymbol{F}_{2k},\ \boldsymbol{W}_{RF}],\ \max_{n\in\{1,\ldots,N_{sub}\}} \left(\sum_{k=1}^{K}\left\|\left(\boldsymbol{W}_{RF}^{H}\boldsymbol{G}_k[n]\boldsymbol{F}_{2k}\right)\right\|_F^2\right)\\
&\quad s.t.\ Tr\left\{\boldsymbol{F}_k[n]\left((\boldsymbol{H}_k[n]\boldsymbol{F}_{RF}\boldsymbol{F}_{BB}[n])\right.\right.\\
&\quad \left.(\boldsymbol{H}_k[n]\boldsymbol{F}_{RF}\boldsymbol{F}_{BB}[n])^H + \sigma_r^2\boldsymbol{I}_{N_r}\right)\\
&\quad \left.\boldsymbol{F}_k^H[n]\right\} \le P_{r,k},\ \forall, k, n,\\
&\quad |\boldsymbol{F}_{2k}(x,y)| = \frac{1}{\sqrt{N_r}},\ |\boldsymbol{W}_{RF}(x,y)|\\
&\quad = \frac{1}{\sqrt{N_d}}, \forall\, x, y.
\end{aligned} \tag{22}$$

It is mathematically challenging to directly solve the problems defined in (21) and (22) for deriving the phase-only processing components. To obtain a feasible solution, an alternating optimization strategy is adopted, where one optimization variable is evaluated while keeping the other fixed. Following this strategy, the aforementioned sub-problems can be solved by finding the common analog precoder at the source $\boldsymbol{F}_{RF}$ and the common RF combiner at the destination $\boldsymbol{W}_{RF}$ by exploiting the notion of tensor decomposition with the assumption that the corresponding phase-only processing components at the k^{th} relay node are known. After finding $\boldsymbol{F}_{RF}$ and $\boldsymbol{W}_{RF}$, the RF beamforming solution at the k^{th} relay station can be obtained by harvesting the array gain.

B. ANALOG BEAMFORMING AT SOURCE AND DESTINATION

Considering N_{sub} sub-carriers, the first-hop channel $\boldsymbol{H}[n] = \left[\boldsymbol{H}_1^T[n], \ldots, \boldsymbol{H}_K^T[n]\right]^T \in \mathbb{C}^{KN_r \times N_t}$ and the second-hop channel $\boldsymbol{G}[n] = [\boldsymbol{G}_1[n], \ldots, \boldsymbol{G}_K[n]] \in \mathbb{C}^{N_d \times KN_r}$ can be represented as $\boldsymbol{H}_{SR} \in \mathbb{C}^{KN_r \times N_t \times N_{sub}}$ and $\boldsymbol{H}_{RD} \in \mathbb{C}^{N_d \times KN_r \times N_{sub}}$, respectively. The tensor decomposition of $\boldsymbol{H}_{SR}$ is given as [42]

$$\boldsymbol{H}_{SR} = \boldsymbol{S}_1 \times_1 \boldsymbol{A}_{(1)} \times_2 \boldsymbol{A}_{(2)} \times_3 \boldsymbol{A}_{(3)}, \tag{23}$$

where $\boldsymbol{S}_1 \in \mathbb{C}^{KN_r \times N_t \times N_{sub}}$ is a core tensor and, $\boldsymbol{A}_{(1)} \in \mathbb{C}^{KN_r \times KN_r}$, $\boldsymbol{A}_{(2)} \in \mathbb{C}^{N_t \times N_t}$ and $\boldsymbol{A}_{(3)} \in \mathbb{C}^{N_{sub} \times N_{sub}}$ are unitary matrices comprising of orthonormal basis. In particular, $\boldsymbol{A}_{(2)}$ consists of orthonormal basis for the column space spanned by

$$\boldsymbol{H}_1 = \left[\left(\boldsymbol{H}_{SR}^{[1]}\right)^T, \left(\boldsymbol{H}_{SR}^{[2]}\right)^T, \ldots, \left(\boldsymbol{H}_{SR}^{[N_{sub}]}\right)^T\right]. \tag{24}$$

By applying SVD on $\boldsymbol{H}_1 \in \mathbb{C}^{N_t \times KN_rN_{sub}}$, the unconstrained beamformer $\boldsymbol{F}_{tmp} \in \mathbb{C}^{N_t \times N_t^{RF}}$ common to all sub-carriers can be obtained by selecting first N_t^{RF} columns of $\boldsymbol{A}_{(2)}$. For instance, $\boldsymbol{H}_1 = \boldsymbol{U}_1\boldsymbol{\Sigma}_1\boldsymbol{V}_1^H$, $\boldsymbol{A}_{(2)} = \boldsymbol{U}_1$ and $\boldsymbol{F}_{tmp}$ can be derived as

$$\begin{aligned}
\boldsymbol{F}_{tmp} &= \boldsymbol{A}_{(2)}\left(:, 1 : N_t^{RF}\right) \\
&= \begin{bmatrix} r_{11}e^{j\theta_{11}} & \cdots & r_{1N_t^{RF}}e^{j\theta_{1N_t^{RF}}} \\ \vdots & \ddots & \vdots \\ r_{N_t1}e^{j\theta_{N_t1}} & \cdots & r_{N_tN_t^{RF}}e^{j\theta_{N_tN_t^{RF}}} \end{bmatrix}.
\end{aligned} \tag{25}$$

It is worthwhile to mention that the computational cost in finding SVD of $\boldsymbol{H}_1$ is unaffordable in practice due to its

large dimensions. Therefore, it is desired to reduce the implementation complexity in determining $\boldsymbol{A}_{(2)}$, which can also be derived from eigen decomposition of $[\boldsymbol{H}_1\boldsymbol{H}_1{}^H] \in \mathbb{C}^{N_t \times N_t}$. Moreover, the beamforming matrix in (25) is infeasible in actual practice due to the absence of element-wise constant amplitude constraint. Hence, the required analog RF beamformer is given as

$$\boldsymbol{F}_{RF} = \left(\frac{1}{\sqrt{N_t}}\right) \begin{bmatrix} e^{jX_{11}} & \dots & e^{jX_{1N_t^{RF}}} \\ \vdots & \ddots & \vdots \\ e^{jX_{N_t1}} & \dots & e^{jX_{N_tN_t^{RF}}} \end{bmatrix}. \tag{26}$$

It is desirable to transform (25) in the form of (26) for designing the analog beamforming solution at the source. Unfortunately, it is quite a challenging task to complete this transformation without avoiding error due to the associated constant modulus constraint. In this scenario, an endeavor is made to minimize the reconstruction loss between (25) and (26) to find the required phase-shift values. For this purpose, the optimization problem that can lead to the minimum reconstruction error is formulated as

$$\min_{\boldsymbol{F}_{RF}} \left\|\boldsymbol{F}_{tmp} - \boldsymbol{F}_{RF}\right\|_F^2 = Tr\left\{\left(\boldsymbol{F}_{tmp} - \boldsymbol{F}_{RF}\right)\left(\boldsymbol{F}_{tmp} - \boldsymbol{F}_{RF}\right)^H\right\}$$
$$|\boldsymbol{F}_{RF}(x,y)| = \frac{1}{\sqrt{N_t}}, \forall\, x, y. \tag{27}$$

It is possible to reduce (27) into a simplified form as

$$\min_{\boldsymbol{F}_{RF}} \sum_{i=1}^{N_t^{RF}} \left(\boldsymbol{F}_{tmp}(:,i) - \boldsymbol{F}_{RF}(:,i)\right)\left(\boldsymbol{F}_{tmp}(:,i) - \boldsymbol{F}_{RF}(:,i)\right)^H$$
$$|\boldsymbol{F}_{RF}(x,y)| = \frac{1}{\sqrt{N_t}}, \forall\, x, y, \tag{28}$$

where $\boldsymbol{F}_{tmp}(:,i) \in \mathbb{C}^{N_t \times 1}$ and $\boldsymbol{F}_{RF}(:,i) \in \mathbb{C}^{N_t \times 1}$ are the i^{th} column of full complexity beamformer and the required constant modulus precoder, respectively. Using (25) and (26), $\boldsymbol{F}_{tmp}(:,i)$ and $\boldsymbol{F}_{RF}(:,i)$ can be written as

$$\boldsymbol{F}_{tmp}(:,i) = \begin{bmatrix} r_{1i}e^{j\theta_{1i}} \\ r_{2i}e^{j\theta_{2i}} \\ \vdots \\ r_{N_ti}e^{j\theta_{N_ti}} \end{bmatrix} \text{ and } \boldsymbol{F}_{RF}(:,i) = \left(\frac{1}{\sqrt{N_t}}\right) \begin{bmatrix} e^{jX_{1i}} \\ e^{jX_{2i}} \\ \vdots \\ e^{jX_{N_ti}} \end{bmatrix}.$$

Therefore, the objective function in (28) can be further decomposed into its simple components as

$$\min_{X_{mi}} \sum_{i=1}^{N_t^{RF}} \sum_{m=1}^{N_t} \left(r_{mi}e^{j\theta_{mi}} - e^{jX_{mi}}\right)\left(r_{mi}e^{j\theta_{mi}} - e^{jX_{mi}}\right)^H$$
$$|\boldsymbol{F}_{RF}(x,y)| = \frac{1}{\sqrt{N_t}}, \forall\, x, y. \tag{29}$$

$$Tr\left\{\boldsymbol{A}[n]\boldsymbol{A}^H[n]\right\} = \left\|\sum_{k=1}^{K} \boldsymbol{W}_{BB}^H[n]\boldsymbol{W}_{RF}^H\boldsymbol{G}_k[n]\boldsymbol{F}_{2k}\boldsymbol{G}_{BB2,k}[n]\boldsymbol{G}_{BB1,k}^H[n]\boldsymbol{F}_{1k}^H\boldsymbol{H}_k[n]\boldsymbol{F}_{RF}\boldsymbol{F}_{BB}[n]\right\|_F^2, \tag{14}$$

$$\leq \sum_{k=1}^{K} \left\|\left(\boldsymbol{W}_{BB}^H[n]\boldsymbol{W}_{RF}^H\boldsymbol{G}_k[n]\boldsymbol{F}_{2k}\boldsymbol{G}_{BB2,k}[n]\right)\left(\boldsymbol{G}_{BB1,k}^H[n]\boldsymbol{F}_{1k}^H\boldsymbol{H}_k[n]\boldsymbol{F}_{RF}\boldsymbol{F}_{BB}[n]\right)\right\|_F^2. \tag{15}$$

$$\leq \sum_{k=1}^{K} \left\{\left\|\left(\boldsymbol{W}_{BB}^H[n]\boldsymbol{W}_{RF}^H\boldsymbol{G}_k[n]\boldsymbol{F}_{2k}\boldsymbol{G}_{BB2,k}[n]\right)\right\|_F^2 \left\|\left(\boldsymbol{G}_{BB1,k}^H[n]\boldsymbol{F}_{1k}^H\boldsymbol{H}_k[n]\boldsymbol{F}_{RF}\boldsymbol{F}_{BB}[n]\right)\right\|_F^2\right\}. \tag{16}$$

$$\leq \left(\sum_{k=1}^{K} \left\|\left(\boldsymbol{W}_{BB}^H[n]\boldsymbol{W}_{RF}^H\boldsymbol{G}_k[n]\boldsymbol{F}_{2k}\boldsymbol{G}_{BB2,k}[n]\right)\right\|_F^2\right)\left(\sum_{k=1}^{K} \left\|\left(\boldsymbol{G}_{BB1,k}^H[n]\boldsymbol{F}_{1k}^H\boldsymbol{H}_k[n]\boldsymbol{F}_{RF}\boldsymbol{F}_{BB}[n]\right)\right\|_F^2\right). \tag{17}$$

$$= \left(\sum_{k=1}^{K} \left\|\left(\boldsymbol{W}_{RF}^H\boldsymbol{G}_k[n]\boldsymbol{F}_{2k}\right)\right\|_F^2\right)\left(\sum_{k=1}^{K} \left\|\left(\boldsymbol{F}_{1k}^H\boldsymbol{H}_k[n]\boldsymbol{F}_{RF}\right)\right\|_F^2\right). \tag{18}$$

$$Tr\left\{\boldsymbol{A}[n]\boldsymbol{A}^H[n]\right\} \approx \left(\sum_{k=1}^{K} \left\|\left(\boldsymbol{W}_{RF}^H\boldsymbol{G}_k[n]\boldsymbol{F}_{2k}\right)\right\|_F^2\right)\left(\sum_{k=1}^{K} \left\|\left(\boldsymbol{F}_{1k}^H\boldsymbol{H}_k[n]\boldsymbol{F}_{RF}\right)\right\|_F^2\right). \tag{19}$$

$$\max_{[\boldsymbol{F}_{RF},\ \boldsymbol{F}_{2k},\ \boldsymbol{F}_{1k},\ \boldsymbol{W}_{RF}]} \left(\sum_{k=1}^{K} \left\|\left(\boldsymbol{W}_{RF}^H\boldsymbol{G}_k[n]\boldsymbol{F}_{2k}\right)\right\|_F^2\right)\left(\sum_{k=1}^{K} \left\|\left(\boldsymbol{F}_{1k}^H\boldsymbol{H}_k[n]\boldsymbol{F}_{RF}\right)\right\|_F^2\right)$$
$$s.t.\ \|\boldsymbol{F}_{RF}\boldsymbol{F}_{BB}[n]\|_F^2 \leq P_s,$$
$$Tr\left\{\boldsymbol{F}_k[n]\left(\left(\boldsymbol{H}_k[n]\boldsymbol{F}_{RF}\boldsymbol{F}_{BB}[n]\right)\left(\boldsymbol{H}_k[n]\boldsymbol{F}_{RF}\boldsymbol{F}_{BB}[n]\right)^H + \sigma_r^2\boldsymbol{I}_{N_r}\right)\boldsymbol{F}_k^H[n]\right\} \leq P_{r,k},\ \forall, k, n,$$
$$|\boldsymbol{F}_{RF}(x,y)| = \frac{1}{\sqrt{N_t}}, |\boldsymbol{F}_{1k}(x,y)| = \frac{1}{\sqrt{N_r}}, |\boldsymbol{F}_{2k}(x,y)| = \frac{1}{\sqrt{N_r}}, \ |\boldsymbol{W}_{RF}(x,y)| = \frac{1}{\sqrt{N_d}}, \forall\, x, y. \tag{20}$$

After simple manipulation, the optimization problem (29) can be transformed into the following form:

$$\min_{X_{mi}} \sum_{i=1}^{N_t^{RF}} \sum_{m=1}^{N_t} \left\{1 + r_{mi}^2 - r_{mi} e^{j(\theta_{mi} - X_{mi})} - r_{mi} e^{-j(\theta_{mi} - X_{mi})}\right\}$$
$$|\boldsymbol{F}_{RF}(x, y)| = \frac{1}{\sqrt{N_t}}, \forall x, y. \tag{30}$$

It is obvious from the objective function that the optimal solution to minimize (30) can be obtained for designing the required RF beamformer at the source when $\theta_{mi} = X_{mi}\ \forall i, m$. Moreover, the obtained result also indicates the condition for deriving the analog beamforming component from the unconstrained beamforming matrix under minimum mean-squared-error (MMSE). Furthermore, the extracted phase-shift values describe the direction in which beamforming vectors cast maximum energy [47].

$$\boldsymbol{F}_{RF} = \left(\frac{1}{\sqrt{N_t}}\right) exp\left\{j\, arg\left(\boldsymbol{F}_{tmp}\right)\right\}, \tag{31}$$

where $arg(.)$ represents the argument operator. The same procedure is equally applicable to derive the common analog combiner $\boldsymbol{W}_{RF}$ at the destination, and the main design steps are given to avoid repetition. The tensor decomposition of second-hop channel $\boldsymbol{H}_{RD}$, as mentioned earlier, can be expressed as

$$\boldsymbol{H}_{RD} = \boldsymbol{S}_2 \times_1 \boldsymbol{B}_{(1)} \times_2 \boldsymbol{B}_{(2)} \times_3 \boldsymbol{B}_{(3)}, \tag{32}$$

where $\boldsymbol{S}_2 \in \mathbb{C}^{N_d \times KN_r \times N_{sub}}$ is a core tensor, and $\boldsymbol{B}_{(1)} \in \mathbb{C}^{N_d \times N_d}$, $\boldsymbol{B}_{(2)} \in \mathbb{C}^{KN_r \times KN_r}$ and $\boldsymbol{B}_{(3)} \in \mathbb{C}^{N_{sub} \times N_{sub}}$ are unitary matrices consisting of orthonormal basis. Here, $\boldsymbol{B}_{(1)}$ is of prime significance, as it contains orthonormal basis for the column space spanned by

$$\boldsymbol{H}_2 = \left[\boldsymbol{H}_{RD}^{[1]}, \boldsymbol{H}_{RD}^{[2]}, \ldots, \boldsymbol{H}_{RD}^{[N_{sub}]}\right] \in \mathbb{C}^{N_d \times KN_r N_{sub}}. \tag{33}$$

Eigen decomposition of $[\boldsymbol{H}_2 \boldsymbol{H}_2^H] \in \mathbb{C}^{N_d \times N_d}$ is performed to derive $\boldsymbol{B}_{(1)}$ with relatively low computational complexity. Let $\boldsymbol{U}_2 \in \mathbb{C}^{N_d \times N_d}$ be the matrix comprising of eigen vectors such that $\boldsymbol{B}_{(1)} = \boldsymbol{U}_2$, and the unconstrained combining matrix at the destination $\boldsymbol{W}_{tmp} \in \mathbb{C}^{N_d \times N_d^{RF}}$ common to all sub-carriers can be obtained by selecting first N_d^{RF} columns of $\boldsymbol{B}_{(1)}$. Therefore,

$$\boldsymbol{W}_{tmp} = \boldsymbol{B}_{(1)}\left(:, 1 : N_d^{RF}\right), \tag{34}$$

This solution is infeasible for practical implementation that requires element-wise constant modulus constraint. Therefore, the required RF combining matrix using (34) can be designed as

$$\boldsymbol{W}_{RF} = \left(\frac{1}{\sqrt{N_d}}\right) exp\left\{j\, arg\left(\boldsymbol{W}_{tmp}\right)\right\}, \tag{35}$$

C. RF BEAMFORMING AT RELAY NODES

For deriving the phase-only processing components at each relay node, the sub-problems (21) and (22) can be expressed as

$$\begin{aligned}
&[\boldsymbol{F}_{RF},\ \boldsymbol{F}_{1k}],\ \max_{n \in \{1,\ldots,N_{sub}\}} \left(\sum_{k=1}^{K} \left\| \left(\boldsymbol{F}_{1k}^H \boldsymbol{H}_k[n] \boldsymbol{F}_{RF}\right)\right\|_F^2\right) \\
&= \left\| \left(\boldsymbol{F}_{11}^H \boldsymbol{H}_1[n] \boldsymbol{F}_{RF}\right)\right\|_F^2 + \ldots \\
&\quad + \left\| \left(\boldsymbol{F}_{1K}^H \boldsymbol{H}_K[n] \boldsymbol{F}_{RF}\right)\right\|_F^2 \\
&s.t.\ \|\boldsymbol{F}_{RF} \boldsymbol{F}_{BB}[n]\|_F^2 \le P_s, \\
&|\boldsymbol{F}_{RF}(x, y)| = \frac{1}{\sqrt{N_t}}, |\boldsymbol{F}_{1k}(x, y)| \\
&= \frac{1}{\sqrt{N_r}}, \forall x, y,
\end{aligned} \tag{36}$$

$$\begin{aligned}
&[\boldsymbol{F}_{2k},\ \boldsymbol{W}_{RF}],\ \max_{n \in \{1,\ldots,N_{sub}\}} \left(\sum_{k=1}^{K} \left\| \left(\boldsymbol{W}_{RF}^H \boldsymbol{G}_k[n] \boldsymbol{F}_{2k}\right)\right\|_F^2\right) \\
&= \left\| \left(\boldsymbol{W}_{RF}^H \boldsymbol{G}_1[n] \boldsymbol{F}_{21}\right)\right\|_F^2 + \ldots \\
&\quad + \left\| \left(\boldsymbol{W}_{RF}^H \boldsymbol{G}_K[n] \boldsymbol{F}_{2K}\right)\right\|_F^2 \\
&s.t.\ Tr\left\{\boldsymbol{F}_k[n] \left((\boldsymbol{H}_k[n] \boldsymbol{F}_{RF} \boldsymbol{F}_{BB}[n])\right.\right. \\
&\quad \left.\left.(\boldsymbol{H}_k[n] \boldsymbol{F}_{RF} \boldsymbol{F}_{BB}[n])^H + \sigma_r^2 \boldsymbol{I}_{N_r}\right) \boldsymbol{F}_k^H[n]\right\} \\
&\le P_{r,k},\ \forall, k, n, \\
&|\boldsymbol{F}_{2k}(x, y)| = \frac{1}{\sqrt{N_r}},\ |\boldsymbol{W}_{RF}(x, y)| \\
&= \frac{1}{\sqrt{N_d}}, \forall x, y.
\end{aligned} \tag{37}$$

It is clear from (36) and (37) that the objective function is the sum of K independent terms as $\boldsymbol{F}_{RF}$ and $\boldsymbol{W}_{RF}$ have already derived. Therefore, it is sufficient to optimize the k^{th} term in both optimization problems for finding the RF beamforming solution at the k^{th} relay node, and the same procedure is exactly valid to design the analog precoder and combiner at any relay station. Hence, the above-mentioned optimization problems can be reduced into the following form:

$$\begin{aligned}
&[\boldsymbol{F}_{RF},\ \boldsymbol{F}_{1k}],\ \max_{n \in \{1,\ldots,N_{sub}\}} \left\| \left(\boldsymbol{F}_{1k}^H \boldsymbol{H}_k[n] \boldsymbol{F}_{RF}\right)\right\|_F^2 \\
&s.t.\ \|\boldsymbol{F}_{RF} \boldsymbol{F}_{BB}[n]\|_F^2 \le P_s, \\
&|\boldsymbol{F}_{RF}(x, y)| = \frac{1}{\sqrt{N_t}}, |\boldsymbol{F}_{1k}(x, y)| \\
&= \frac{1}{\sqrt{N_r}}, \forall x, y,
\end{aligned} \tag{38}$$

$$\begin{aligned}
&[\boldsymbol{F}_{2k},\ \boldsymbol{W}_{RF}],\ \max_{n \in \{1,\ldots,N_{sub}\}} \left\| \left(\boldsymbol{W}_{RF}^H \boldsymbol{G}_k[n] \boldsymbol{F}_{2k}\right)\right\|_F^2 \\
&s.t.\ Tr\left\{\boldsymbol{F}_k[n] \left((\boldsymbol{H}_k[n] \boldsymbol{F}_{RF} \boldsymbol{F}_{BB}[n])\right.\right. (\boldsymbol{H}_k[n] \\
&\quad \left.\left.\boldsymbol{F}_{RF} \boldsymbol{F}_{BB}[n])^H + \sigma_r^2 \boldsymbol{I}_{N_r}\right) \boldsymbol{F}_k^H[n]\right\} \le P_{r,k},
\end{aligned}$$

$$\forall, k, n, |\boldsymbol{F}_{2k}(x, y)| = \frac{1}{\sqrt{N_r}}, \ |\boldsymbol{W}_{RF}(x, y)| = \frac{1}{\sqrt{N_d}}, \forall x, y. \tag{39}$$

The phase-only processing components at the k^{th} relay station i.e., $\boldsymbol{F}_{1k}$ and $\boldsymbol{F}_{2k}$, can be obtained by maximizing $\|\boldsymbol{H}_k[n]\boldsymbol{F}_{RF}\|_F^2$ and $\left\|\boldsymbol{W}_{RF}^H\boldsymbol{G}_k[n]\right\|_F^2$ over the whole frequency spectrum, respectively. Considering this aspect of designing the RF beamforming, the optimization problems can be reduced into the following form:

$$\begin{aligned}
&\max_{n\in\{1,\ldots,N_{sub}\}}\left(\|\boldsymbol{H}_k[n]\boldsymbol{F}_{RF}\|_F^2\right)\\
&s.t.\ \|\boldsymbol{F}_{RF}\boldsymbol{F}_{BB}[n]\|_F^2 \le P_s,\\
&\quad |\boldsymbol{F}_{RF}(x, y)| = \frac{1}{\sqrt{N_t}}, \forall x, y,\\
&\max_{n\in\{1,\ldots,N_{sub}\}}\left(\left\|\boldsymbol{W}_{RF}^H\boldsymbol{G}_k[n]\right\|_F^2\right)\\
&s.t.\ Tr\left\{\boldsymbol{F}_k[n]\left((\boldsymbol{H}_k[n]\boldsymbol{F}_{RF}\boldsymbol{F}_{BB}[n])(\boldsymbol{H}_k[n]\boldsymbol{F}_{RF}\boldsymbol{F}_{BB}[n])^H\right.\right.\\
&\quad \left.\left.+\sigma_r^2\boldsymbol{I}_{N_r}\right)\boldsymbol{F}_k^H[n]\right\} \le P_{r,k}, \ \forall, k, n,\\
&\quad |\boldsymbol{W}_{RF}(x, y)| = \frac{1}{\sqrt{N_d}}, \forall x, y.
\end{aligned} \tag{40, 41}$$

The solutions to the problems (40) and (41) can lead to the design of $\boldsymbol{F}_{1k}$ and $\boldsymbol{F}_{2k}$, respectively. It is worth mentioning that the interest lies in finding $\boldsymbol{F}_{1k}$ and $\boldsymbol{F}_{2k}$ enabling good performance in the presence of channel estimation error and PN in hybrid beamformers. Before moving further, it is significant to describe the inherent feature of the optimization technique that shows robustness even in the presence of error, noise, and other irregularities in the underlying data. Robustness is referred to as resistance to outliers in a dataset. The more able a design is to avoid undesirable values, the more robust it is. Furthermore, it is known that L_1-norm is more robust, against unexpected and irregular values in measurements, than L_2-norm. Note that the Frobenius norm and L_2-norm of a matrix are closely correlated to each other. Keeping this perspective in view, the task of designing the RF processing components can be achieved by converting the objective function in both optimization problems into L_1-norm maximization problems, as the new objective function has a great potential to achieve better results in the presence of outliers or noisy channels. Therefore,

$$\begin{aligned}
&\max_{n\in\{1,\ldots,N_{sub}\}}\left(\|\boldsymbol{H}_k[n]\boldsymbol{F}_{RF}\|_1^2\right)\\
&s.t.\ \|\boldsymbol{F}_{RF}\boldsymbol{F}_{BB}[n]\|_F^2 \le P_s,\\
&\quad |\boldsymbol{F}_{RF}(x, y)| = \frac{1}{\sqrt{N_t}}, \forall x, y,\\
&\max_{n\in\{1,\ldots,N_{sub}\}}\left(\left\|\boldsymbol{W}_{RF}^H\boldsymbol{G}_k[n]\right\|_1^2\right)\\
&s.t.\ Tr\left\{\boldsymbol{F}_k[n]\left((\boldsymbol{H}_k[n]\boldsymbol{F}_{RF}\boldsymbol{F}_{BB}[n])(\boldsymbol{H}_k[n]\boldsymbol{F}_{RF}\boldsymbol{F}_{BB}[n])^H\right.\right.\\
&\quad \left.\left.+\sigma_r^2\boldsymbol{I}_{N_r}\right)\boldsymbol{F}_k^H[n]\right\} \le P_{r,k}, \ \forall, k, n,\\
&\quad |\boldsymbol{W}_{RF}(x, y)| = \frac{1}{\sqrt{N_d}}, \forall x, y.
\end{aligned} \tag{42, 43}$$

Moreover, the reformulated problems based on L_1-norm maximization can achieve performance close to the upper bound defined by full-complexity precoding, provided the rank of the equivalent baseband channels in the first-hop and second-hop is sufficient to support the transmission of the maximum allowable data streams simultaneously [48]. Also, the equivalent channels observed from the baseband processing components harvest array gain, which in turn increases sub-channel gains for multi-stream transmission.

Note that the optimization problems (42) and (43) are still non-convex due to the element-wise constant modulus constraints associated with the RF beamforming matrices. To avoid mathematically intractable situations while solving these problems, the constant amplitude constraint can be relaxed temporarily for the extraction of phase-shift values that lead to the better design of required RF beamforming solution at relay nodes. Specifically, this temporary relaxation strategy may help non-codebook-based methods for finding the optimal phase-shift values, where array gain attains maximum value. In codebook-based hybrid precoding techniques, standard beamforming vectors are already available in the dictionary matrix for the proper choice of phase-only processing components. Therefore, the problems (42) and (43) without constant amplitude constraints are given as

$$\begin{aligned}
\boldsymbol{H}_{tmp1} &= \max\left(\left\|\boldsymbol{H}_k[n]\boldsymbol{F}_{tmp}\right\|_1\right), \ \forall n\in\{1, \ldots, N_{sub}\}\\
&\quad s.t.\ \|\boldsymbol{F}_{RF}\boldsymbol{F}_{BB}[n]\|_F^2 \le P_s,
\end{aligned} \tag{44}$$

$$\begin{aligned}
\boldsymbol{H}_{tmp2} &= \max\left(\left\|\boldsymbol{W}_{tmp}^H\boldsymbol{G}_k[n]\right\|_1\right), \ \forall n\in\{1, \ldots, N_{sub}\}\\
&\quad s.t.\ Tr\{\boldsymbol{F}_k[n]((\boldsymbol{H}_k[n]\boldsymbol{F}_{RF}\boldsymbol{F}_{BB}[n])(\boldsymbol{H}_k[n]\\
&\qquad \boldsymbol{F}_{RF}\boldsymbol{F}_{BB}[n])^H+\sigma_r^2\boldsymbol{I}_{N_r})\boldsymbol{F}_k^H[n]\} \le P_{r,k},\\
&\quad \forall, k, n.
\end{aligned} \tag{45}$$

While solving the problem (44), it is required to find the RF combiner $\boldsymbol{F}_{1k}$ common to all sub-carriers at the k^{th} relay station. To achieve this target, an iterative method is followed that leads to the unconstrained beamforming matrix, which can be employed to drive the required phase-only combiner. Let $\boldsymbol{H}_{tmp1}$ be the solution of the optimization problem (44) that gives maximum gain of the effective baseband channel $\boldsymbol{F}_{1k}^H\boldsymbol{H}_k[n]\boldsymbol{F}_{RF}$ over all frequency-carriers. Therefore,

$$max\left|\boldsymbol{F}_{1k}^H\boldsymbol{H}_k[n]\boldsymbol{F}_{RF}\right|, \forall n = \boldsymbol{F}_{1k}^H\boldsymbol{H}_{tmp1}. \tag{46}$$

The above formulation has the same form as that of equal gain transmission (EGT) method in [48] with phase-only precoding to harvest the large array gain. It is accomplished by extracting the element-wise phase of $\boldsymbol{H}_{tmp1}$ that can be considered as a useful approach in obtaining the performance close to the theoretical upper bound. Hence, the common RF combiner at the k^{th} relay node $\boldsymbol{F}_{1k}$ can be evaluated as

$$\boldsymbol{F}_{1k} = \left(\frac{1}{\sqrt{N_r}}\right)e^{jarg(\boldsymbol{H}_{tmp1})}, \tag{47}$$

where $\left(\frac{1}{\sqrt{N_r}}\right)$ is the power normalization factor. It is worth highlighting that EGT technique in MIMO communication for deriving the phase-only processing component is valid only when equal number of RF chains is deployed on both sides of a communication link. When this condition is satisfied then $\boldsymbol{F}_{1k}^{H}\boldsymbol{H}_k[n]\boldsymbol{F}_{RF}$ must be a square matrix and diagonal elements represent sub-channel gains. The non-zero off-diagonal elements show inter-chain interference, which can be eliminated by indirect method as discussed in the forthcoming baseband precoding section. Similarly, the RF precoder at the k^{th} relay station $\boldsymbol{F}_{2k}$ can be derived by solving the optimization problem (45). Let $\boldsymbol{H}_{tmp2}$ be the solution of the problem (45) corresponding to the maximum gain of the effective baseband channel $\boldsymbol{W}_{RF}^{H}\boldsymbol{G}_k[n]\boldsymbol{F}_{2k}$ over the allocated frequency spectrum. The formulation of the problem (45) for designing $\boldsymbol{F}_{2k}$ by exploiting the notion of EGT is given as

$$max\left|\boldsymbol{W}_{RF}^{H}\boldsymbol{G}_k[n]\boldsymbol{F}_{2k}\right|, \forall n = \boldsymbol{H}_{tmp2}\boldsymbol{F}_{2k}\,, \tag{48}$$

Just like (44), the element-wise phase-extraction of $\boldsymbol{H}_{tmp2}$ can facilitate in obtaining the required RF precoding matrix $\boldsymbol{F}_{2k}$ as

$$\boldsymbol{F}_{2k} = \left(\frac{1}{\sqrt{N_r}}\right)e^{jarg\left(\boldsymbol{H}_{tmp2}^{H}\right)}, \tag{49}$$

IV. DIGITAL BASEBAND PRECODING

After designing the analog RF beamforming at communicating nodes, it is required to derive the corresponding baseband processing components at different frequency-carriers to complete the hybrid transceiver design. To achieve this target, SVD is performed on the equivalent baseband channels in the first-hop $\boldsymbol{H}_{eq}^{k}[n] = \boldsymbol{F}_{1k}^{H}\boldsymbol{H}_k[n]\boldsymbol{F}_{RF}$ and second-hop $\boldsymbol{G}_{eq}^{k}[n] = \boldsymbol{W}_{RF}^{H}\boldsymbol{G}_k[n]\boldsymbol{F}_{2k}$. This process enables to find the orthonormal digital precoder and combiner at the k^{th} relay node corresponding to the n^{th} frequency sub-carrier. As $\boldsymbol{H}_{eq}^{k}[n] = \boldsymbol{U}_{SR,k}[n]\boldsymbol{\Sigma}_{SR,k}[n]\boldsymbol{V}_{SR,k}^{H}[n]$ and $\boldsymbol{G}_{eq}^{k}[n] = \boldsymbol{U}_{RD,k}[n]\boldsymbol{\Sigma}_{RD,k}[n]\boldsymbol{V}_{RD,k}^{H}[n]$ and therefore, the optimal baseband precoder $\boldsymbol{G}_{BB2,k}[n]$ and combiner $\boldsymbol{G}_{BB1,k}[n]$ at the k^{th} relay station, on a per sub-carrier basis, can be obtained by taking the N_s column vectors of $\boldsymbol{V}_{RD,k}[n]$ and $\boldsymbol{U}_{SR,k}[n]$, respectively, corresponding to the N_s largest singular values. Hence,

$$\begin{aligned}\boldsymbol{G}_{BB1,k}[n] &= \boldsymbol{U}_{SR,k}[n](:, 1:N_s)\,,\\ \boldsymbol{G}_{BB2,k}[n] &= \boldsymbol{V}_{RD,k}[n](:, 1:N_s)\,.\end{aligned} \tag{50}$$

Now, it is possible to define the equivalent baseband channel from the source to the destination for designing the optimal digital precoder $\boldsymbol{F}_{BB}[n]$ and combiner $\boldsymbol{W}_{BB}[n]$, respectively, as

$$\boldsymbol{H}_{SD,eq}[n] = \boldsymbol{W}_{RF}^{H}\boldsymbol{G}[n]\boldsymbol{F}[n]\boldsymbol{H}[n]\boldsymbol{F}_{RF} \in \mathbb{C}^{N_d^{RF}\times N_t^{RF}}. \tag{51}$$

The equivalent channel in (51) can be expressed as $\boldsymbol{H}_{SD,eq}[n] = \boldsymbol{U}_{SD}[n]\boldsymbol{\Sigma}_{SD}[n]\boldsymbol{V}_{SD}^{H}[n]$ and the required baseband processing components are obtained by taking the N_s column vectors of $\boldsymbol{V}_{SD}[n]$ and $\boldsymbol{U}_{SD}[n]$. Therefore,

$$\boldsymbol{F}_{BB}[n] = \boldsymbol{V}_{SD}[n](:, 1:N_s)\,, \boldsymbol{W}_{BB}[n] = \boldsymbol{U}_{SD}[n](:, 1:N_s)\,. \tag{52}$$

This design strategy, for deriving the low-dimensional digital precoders and combiner, minimizes interference among transmitted data streams indirectly.

A. EFFECT OF PHASE NOISE

To improve the robustness of the proposed design, another imperfection in the hybrid beamforming matrices, i.e., PN, is taken into consideration. Note that PN is modeled with two independent contributions at the source and destination. Moreover, the hybrid beamforming matrix after including the effect of PN can be obtained through multiplication of the diagonal matrix. This process induces errors in the phase-shift values of the hybrid processing matrices. For instance, the PN matrix $\boldsymbol{M}_{PN}^{T}\in\mathbb{C}^{N_t^{RF}\times N_t^{RF}}$ at the source that acts between $\boldsymbol{F}_{BB}[n]$ and $\boldsymbol{F}_{RF}$ is given as

$$\boldsymbol{M}_{PN}^{T} = diag\left(e^{j\emptyset_{T,1}}, \ldots, e^{j\emptyset_{T,N_t^{RF}}}\right), \tag{52a}$$

where $\emptyset_{T,p}, p\in\{1, .., N_t^{RF}\}$ are zero-mean Gaussian random variables. Similarly, the PN matrix $\boldsymbol{M}_{PN}^{R}\in\mathbb{C}^{N_r^{RF}\times N_r^{RF}}$ at the destination that acts between $\boldsymbol{W}_{BB}[n]$ and $\boldsymbol{W}_{RF}$ is given as

$$\boldsymbol{M}_{PN}^{R} = diag\left(e^{j\varphi_{R,1}}, \ldots, e^{j\varphi_{R,N_r^{RF}}}\right), \tag{52b}$$

where $\varphi_{R,q}, q\in\{1, .., N_r^{RF}\}$ are zero-mean Gaussian random variables. Considering the effect of PN, hybrid precoders at the source and hybrid combiners at the destination can be expressed as $\left(\boldsymbol{F}_{BB}[n]\boldsymbol{M}_{PN}^{T}\boldsymbol{F}_{RF}\right)$ and $\left(\boldsymbol{W}_{BB}[n]\boldsymbol{M}_{PN}^{R}\boldsymbol{W}_{RF}\right)$, respectively.

V. COMPUTATIONAL COMPLEXITY

In the previous sections, the hybrid wideband transceiver design was proposed for achievable rate maximization in multi-relay MIMO systems. Tensor decomposition was employed to derive the common orthonormal beamforming vectors at the source and destination over the allocated frequency band, and then the reconstruction loss minimization problem was formulated for the extraction of optimal phase values under the MMSE criterion. In this case, the computational complexity for finding the required phase-shift values is in the order of $O(MN_tN_rN_{sub})$, $M := \max\{N_tN_rN_{sub}\}$. Moreover, the computational cost for finding the solution of $\max_n \left\|\boldsymbol{W}_{RF}^{H}\boldsymbol{G}_k[n]\right\|_1^2$, $n\in\{1, 2, \ldots, N_{sub}\}$ is in the order of $O(N_d^{RF}N_rN_d)$. Therefore, the complexity for deriving the phase-only beamforming solution is given as

$$\begin{aligned}Z_1 &= N_t^2N_rN_{sub} + N_d^{RF}N_rN_d\\ &= N_r\left(N_t^2N_{sub} + N_r^{RF}N_d\right).\end{aligned} \tag{53}$$

The computational cost, for deriving the baseband beamformers, is in the order of $O\left(N_s^3\right)$. Finally, the overall complexity of the proposed algorithm can be approximated by the

TABLE 1. Complexity expressions of the proposed and the other hybrid precoding designs.

Algorithms	Complexity
Proposed	$N_r(N_t^2 N_{sub} + N_r^{RF} N_d) + N_s^3$
Hybrid Precoding [25]	$N_s^4 + N_s^3(N_t + N_r) + (N_t N_r N_s)^2 + N_{sub}(N_s^3 + N_t^2 N_r + N_r^2 N_s)$
Hybrid Beamforming [49]	$N_{sub}\left(N_s^3 + N_t^2 N_r + N_t\left({N_s}^2 + {N_r}^2\right)\right) + N_s({N_t}^2 + {N_r}^2)$

following expression as

$$Z_1^{tot} \approx N_r \left(N_t^2 N_{sub} + N_r^{RF} N_d\right) + N_s^3. \tag{54}$$

It is required to compare the computational complexity of the proposed scheme with other hybrid beamforming algorithms, as this comparison helps highlight the usefulness of the proposed algorithm. Table 1 summarizes the complexity expressions of the proposed approach and the hybrid precoding algorithms presented in [25] and [49]. Fig. 2 illustrates the complexity of the proposed algorithm compared with hybrid precoding techniques given in [25] and [49] as a function of the number of antennas deployed at communicating nodes. To generate simulation results, 64 sub-carriers are taken into account with $N_t^{RF} = N_r^{RF} = N_d^{RF} = N_s = 4$. It is evident from the obtained results that the computational cost of the proposed hybrid transceiver is less than the algorithms given in [25] and [49]. In particular, the complexity of the presented technique is approximately two times lower than the hybrid precoding design in [49]. Table 2 provides numerical data that describes the low-complexity profile of the proposed scheme as a function of the number of antennas at communicating nodes. For instance, the computational burden of the proposed method is approximately 26 times less than the hybrid precoding design in [25] when 100 antennas are considered at communicating nodes. Similarly, the computational cost is nearly 50 times less than the hybrid beamforming design in [25] when 196 antennas are deployed at communicating units.

VI. SIMULATION RESULTS

In this section, computer simulations are conducted to demonstrate the performance of the proposed hybrid precoding. Table 3 shows the main simulation parameters without considering the spatial wideband effect, and Table 4 depicts system parameters for simulation when the beam squint effect is taken into account. The relay nodes in the underlying system are spatially distributed; therefore, interference among the channels from the source to the relay nodes can be ignored. Moreover, it is assumed that relay nodes are deployed at approximately equal distances from the source and destination. Hence, channel statistics remain

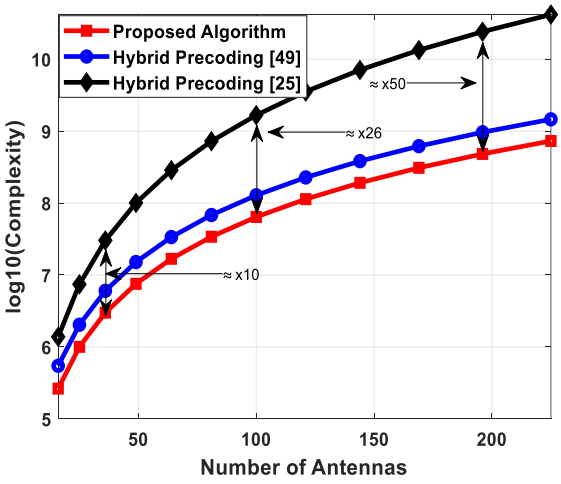

FIGURE 2. Computational complexity vs. number of antennas with 64 sub-carriers. Proposed scheme compared with other hybrid beamforming algorithms when $N_s = 4$. The number of RF chains is equal to the number of data streams.

TABLE 2. Low complexity profile of the proposed design.

$N_t = N_r = N_d$	Algorithm in [49]	Algorithm in [25]
16	2.08	5.25
25	2.03	7.34
36	2.01	10.09
49	2.00	13.32
64	2.00	17.05
81	2.00	21.28
100	2.00	26.02
121	2.00	31.27
144	2.00	37.02
169	2.00	43.26
196	2.00	50.00
225	2.00	57.25

the same under this deployment strategy. In addition, 64 sub-carriers (IEEE 802.11a WLAN) are considered as in [50], but the proposed approach works for any arbitrary number of sub-carriers (e.g., 128, 256, etc.). All the simulation results are averaged over 500 channel realizations. The frequency domain description of mm-Wave channel for the n^{th} sub-carrier $\boldsymbol{H}_{mm-wave}[n] \in \mathbb{C}^{N_r \times N_t}$ is given as [26]

$$\boldsymbol{H}_{mm-wave}[n] = \sqrt{\frac{N_t N_r}{N_{cl} N_{ray}}} \sum_{i=0}^{N_{cl}-1} \sum_{l=1}^{N_{ray}} \alpha_{il} \boldsymbol{a}_r\left(\varphi_{il}^r, \theta_{il}^r\right) \boldsymbol{a}_t\left(\varphi_{il}^t, \theta_{il}^t\right)^H e^{-j2\pi \frac{i.n}{N_{sub}}}, \tag{55}$$

where N_{cl} and N_{ray} are the number of clusters and the number of data transmission paths per cluster, respectively. α_{il} denotes the complex gain of the l^{th} propagation path in the i^{th} cluster such that $\alpha_{il} \sim \mathcal{CN}(0, \sigma_{\alpha,i}^2)$, $\boldsymbol{a}_t\left(\varphi_{il}^t, \theta_{il}^t\right)$ and $\boldsymbol{a}_r\left(\varphi_{il}^r, \theta_{il}^r\right)$ are the transmit and receive array response vectors,

TABLE 3. System parameters for simulation without beam squint.

Parameters	Values
Number of antennas	$N_t = N_r = N_d = 16{\sim}225$
Number of data streams	$N_s = 4{\sim}12$
Number of RF chains	$N_t^{RF} = N_r^{RF} = N_d^{RF} = N_s$
Number of sub-carriers	$N_{sub} = 64$
Number of propagation paths	$N_{cl} = 3, N_{ray} = 10$
Carrier frequency	$f_c = 28\ GHz$
Number of relay nodes	$K = 1{\sim}8$

respectively, and $(\varphi_{il}^t, \varphi_{il}^r)$ and $(\theta_{il}^t, \theta_{il}^r)$ are the angles of departure (*AoDs*) and the angles of arrival (*AoAs*) in azimuth and elevation, respectively.

A. PERFORMANCE EVALUATION WITH NUMBER OF DATA STREAMS

Fig. 4 shows the spectral efficiency performance of the proposed algorithm, by changing the number of transmitted data streams, i.e., $N_s = \{4, 6, 8\}$, in a mm-Wave propagation environment with uniform planar arrays (UPAs) for the deployment of antennas at different communicating nodes. To generate simulation results, the number of antennas at the source, each relay node and the destination are set as $N_t = N_r = N_d = 100$, respectively. The mm-Wave channel matrix, corresponding to different frequency-carriers, is generated according to (55), where channel parameters are initialized as $N_{ray} = 10$, $N_{cl} = 3$, $\sigma_{\alpha,i}^2 = 1\ \forall i$, and $AS = 10^o$ that describe the number of rays/cluster with Laplacian distributed azimuth and elevation angles of arrival and departure, number of clusters, average power of each cluster and standard deviation, respectively. It is worth mentioning that the number of RF chains is equal to the number of data streams, i.e., $N_t^{RF} = N_r^{RF} = N_d^{RF} = N_s$ for the evaluation of the achievable rate. Moreover, the number of RF chains cannot be less than N_s according to the essential condition that hybrid beamforming needs to follow, as mentioned in Section II. The spectral efficiency achieved by the proposed scheme is compared with full-complexity precoding under two main conditions associated with CSI such as (a) perfect CSI (b) imperfect CSI with different levels of accuracy.

It is obvious from the obtained results that there is a small performance gap between the proposed approach and fully digital precoding under the assumption of perfect CSI, but degradation in the performance occurs when the estimated channel with a different accuracy factor is taken into account. For instance, the performance of the proposed hybrid beamforming is close to that of perfect CSI when $\delta = 0.9$, and the performance gap increases by decreasing the value of δ such as 0.8 and 0.7. It is also clear from Fig. 4 that the proposed method achieves nearly consistent performance over a range of transmitted data streams.

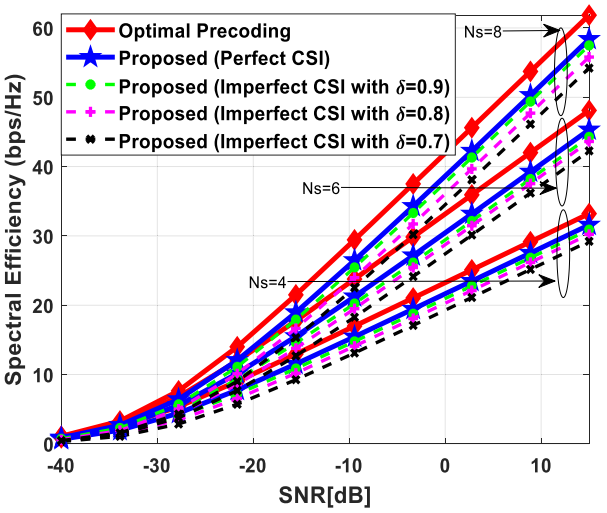

FIGURE 3. Spectral efficiency vs. SNR when $N_t = N_r = N_d = 100$ and $N_s = \{4, 6, 8\}$. It is assumed that 2 relay stations are deployed between the source and destination. The mm-Wave propagation environment is described by the following parameters channels $N_{cl} = 3$, $N_{ray} = 10$ and 10^o spread angle to generate channel matrix for different sub-carriers.

B. EFFECT OF PHASE NOISE ON PERFORMANCE

Fig. 5 illustrates the impact of phase noise (PN) on the performance of the proposed hybrid beamforming technique (a) when estimated channel with $\delta = 0.8$ is employed, and (b) PN is incorporated at the transmitter and receiver using (52a) and (52b). To generate simulation results, the number of antennas at different communicating nodes are set as $N_t = N_r = N_d = 100$ for the transmission of $N_s = \{4, 8\}$ data streams by deploying 2 relay nodes between the source and destination. Moreover, mm-Wave channel parameters are set as $N_{ray} = 10$, $N_{cl} = 3$, $\sigma_{\alpha,i}^2 = 1\ \forall i$, and $AS = 10^o$ to generate channel matrix for different sub-carriers.

It is evident from the obtained results that the performance degradation due to PN is approximately equal to the performance loss when imperfect channel is considered with $\delta = 0.8$. Again, the proposed approach achieves consistent performance in the presence of PN over a range of transmitted data streams.

C. PERFORMANCE EVALUATION BY INCREASING NUMBER OF RELAY NODES

Fig. 6 describes the achievable rate by increasing the number of relay nodes. The system parameters in this case are initialized as $N_t = N_r = N_d = 100$ for the transmission of $N_s = \{6, 8\}$ data streams with the deployment of 4 relay nodes between the source and destination. The mm-Wave channel matrix corresponding to different frequency-carriers is generated using (55) with these channel parameters $N_{ray} = 10$, $N_{cl} = 3$, $\sigma_{\alpha,i}^2 = 1\ \forall i$, and $AS = 10^o$. In addition to the increase in spectral efficiency, the obtained results follow a

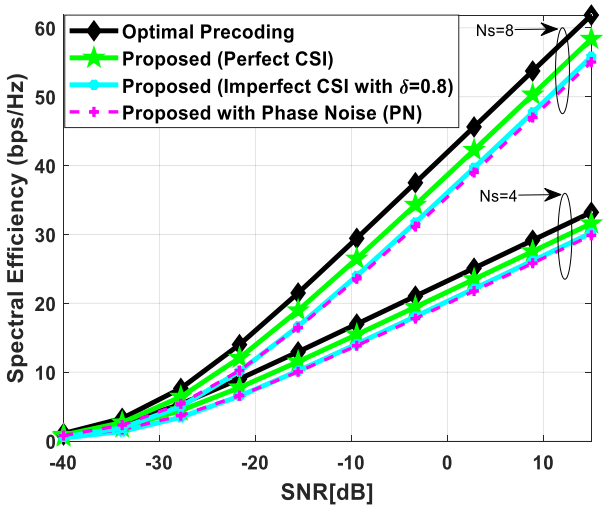

FIGURE 4. Spectral efficiency vs. SNR when PN in hybrid beamformers, at the source and destination, is taken into account. The number of antennas and data streams are set as $N_t = N_r = N_d = 100$ and $N_s = \{4,\ 8\}$. There are 2 relay nodes between the transmitter and receiver.

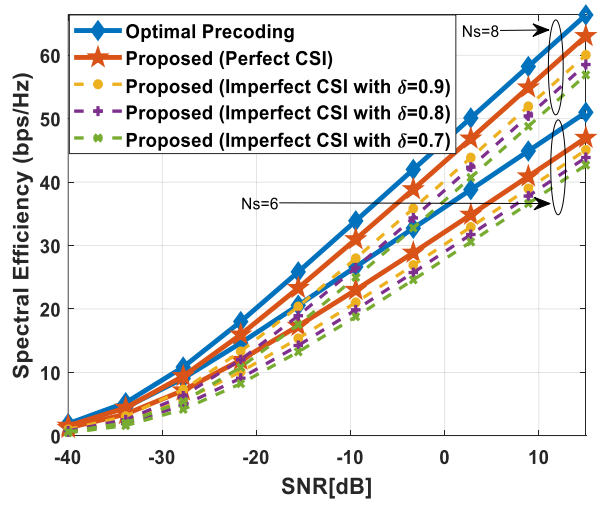

FIGURE 5. Spectral efficiency vs. SNR when $N_t = N_r = N_d = 100$ and $N_s = \{6,\ 8\}$ The mm-Wave channel parameters are initialized as $N_{cl} = 3,\ N_{ray} = 10$ and 10^o spread angle. There are 4 relay nodes deployed between the source and destination to facilitate long-distance transmission.

similar pattern as that of Fig. 4. For instance, the performance of the proposed scheme with 10 % channel estimation error is close to the performance under perfect CSI assumption. There is a gradual decrease in performance when channel estimation error increases 20 % and 30 %, respectively, as shown in Fig. 6.

Fig. 7 describes the impact of PN on the performance of the proposed algorithm by increasing the number of relay nodes. The system parameters and mm-Wave channel parameters are the same as in the previous case for the generation of simulation results. It is obvious from the obtained results that spectral efficiency achieved by the proposed approach in the presence of PN is approximately equal to the performance

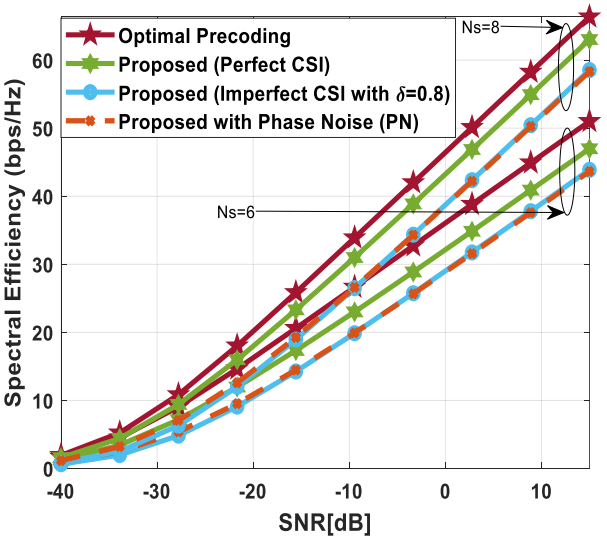

FIGURE 6. Spectral efficiency vs. SNR when PN is considered in hybrid beamforming matrices at the source and destination. The number of antennas and data streams are set as $N_t = N_r = N_d = 100$ and $N_s = \{6,\ 8\}$ There are 4 relay nodes deployed between the transmitter and receiver to enhance the range of communication.

when imperfect channel matrix is generated with $\delta = 0.8$ using (56).

Fig. 8 plots the spectral efficiency by further increasing the number of relay nodes with a relatively small number of antennas at communicating units. In this case, the number of antennas at the source, each relay station, and the destination are set as $N_t = N_r = N_d = 64$ for the transmission of $N_s = \{8,\ 10,\ 12\}$ data streams with the deployment of 6 relay nodes to assist the source transmitted signals. The obtained results clearly show that the spectral efficiency achieved by the proposed method at $\delta = 0.9$ is close to the performance under the perfect CSI assumption. In addition, the performance of the presented approach is evaluated at $\delta = 0.85,\ 0.8$ and the performance degradation occurs in a gradual manner with the increase in channel estimation error, as depicted in Fig. 8. Again, the performance curves obey a similar pattern as in previous cases. This behavior indicates the consistency of the performance and usefulness of the proposed algorithm.

D. PERFORMANCE WITH NUMBER OF ANTENNAS

Fig. 9 plots the spectral efficiency performance of the proposed hybrid beamforming design as a function of the number of antennas at communicating nodes. To show the validity of the proposed scheme for small, medium, and large number of antennas, the number of antennas at the source, each relay station, and the destination are changed over a wide range in a gradual fashion such as $N_t = N_r = N_d = \{16,\ 25,\ 36,\ 49,\ 64,\ 81,\ 100,\ 121,\ 144,\ 169,\ 196,\ 225\}$. The number of data streams is set as $N_s = 12$ and simulation results are obtained by keeping SNR constant at -15, 0, 15 [dB]. Furthermore, there are 4 relay nodes deployed to assist signal transmission from the source to the destination.

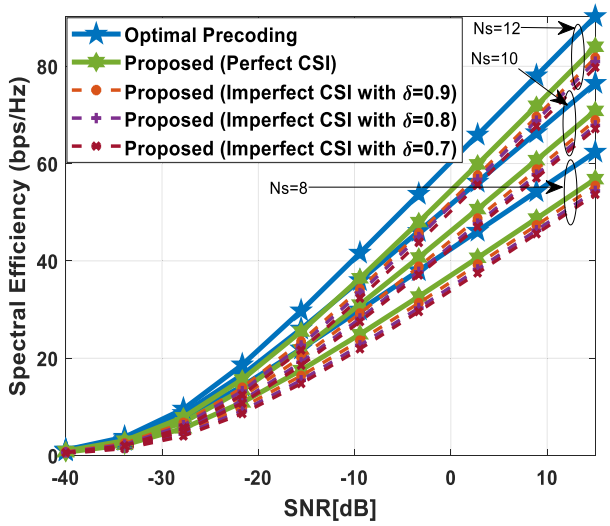

FIGURE 7. Spectral efficiency vs. SNR when $N_t = N_r = N_d = 64$ and $N_s = \{8,\ 10,\ 12\}$There are 6 relay nodes deployed between the transmitter and receiver for efficient data transmission. The mm-Wave channel parameters are set as $N_{cl} = 3,\ N_{ray} = 10$ and 10^o spread angle.

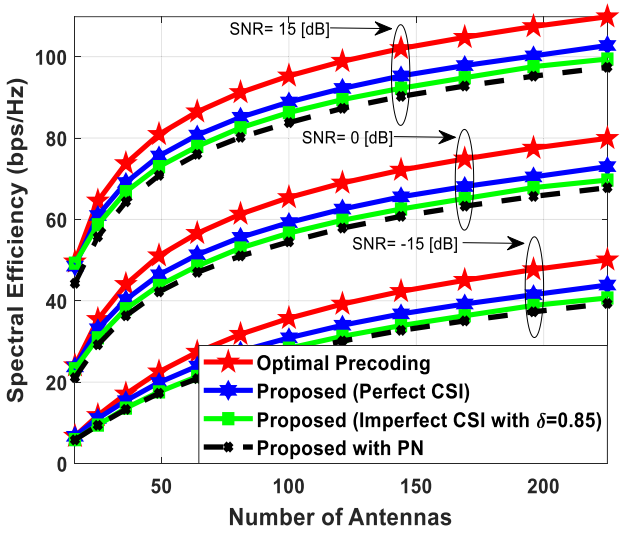

FIGURE 8. Spectral efficiency vs. number of antennas at SNR= -15, 0, 15 [dB]. There are 4 relay stations between the source and destination to assist the transmission of $N_s = 12$ data streams.

It is clear from Fig. 9 that spectral efficiency increases rapidly for a small number of antennas, while a relatively slow increase in spectral efficiency is observed for a number of antennas in medium range. At a large number of antennas, the increase in spectral efficiency becomes significantly low, and this tendency indicates that saturation level is going to be attained. In addition to the consistent performance at different SNR levels, the spectral efficiency achieved at 15% channel estimation error is close to the performance obtained under the CSI assumption. Moreover, there is a negligibly small performance gap when comparison is made between PN and the performance with $\delta = 0.85$.

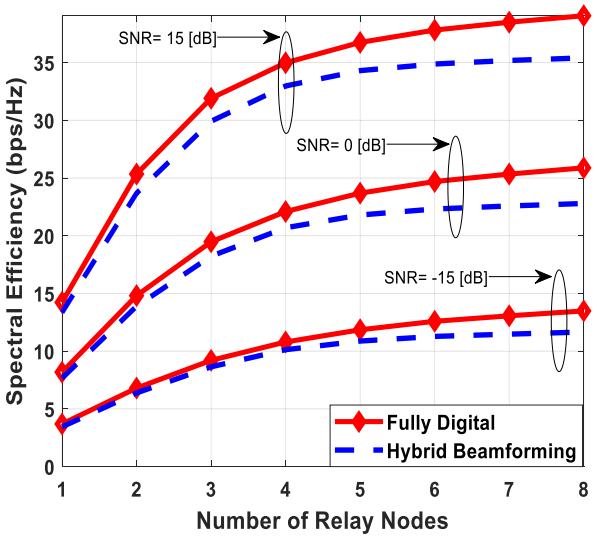

FIGURE 9. Spectral efficiency vs. number of relay nodes at SNR= -15, 0, 15 [dB]. The system parameters are given as $N_t = N_r = N_d = 16$ and $N_s = 10$.

E. PERFORMANCE WITH NUMBER OF RELAY NODES

Fig. 10 illustrates the data transmission rate as a function of the number of relay stations. There are 16 antennas deployed at each communicating node $N_t = N_r = N_d = 16$ for the transmission of a relatively large number of data streams, i.e., $N_s = 10$. The mm-Wave channel parameters are set as in previous cases. It is obvious from the obtained results that the transmission rate significantly increases when a second relay node is deployed between the source and destination. Moreover, the performance curve shows that data transmission rate increases with an increase in relay nodes, but the increase in data rate becomes small in a gradual manner.

When the change in data rate becomes negligibly small by the addition of relay station, the system then enters the saturation level, and this behavior facilitates determining the maximum number of relay nodes that can be deployed to improve the performance.

F. PERFORMANCE COMPARISON WITH OTHER ALGORITHMS

Fig. 11 shows the achievable rate of the proposed algorithm when compared with the other hybrid beamforming techniques. The number of antennas deployed at communicating nodes is set as $N_t = N_r = N_d = 25$ for the transmission of $N_s = 8$ data streams. There are 4 relay nodes between the source and destination to enhance the transmission range, link quality, coverage, and spectral efficiency. The mm-Wave channel parameters are the same as that of the previous cases. Furthermore, it is assumed that the number of RF chains is equal to the number of data streams while generating simulation results. It is clear from the obtained results that the proposed method outperforms when compared to the hybrid precoding techniques in [31] and [35].

G. BEAM SQUINT EFFECT

Fig. 12 depicts the spectral efficiency performance of the proposed hybrid transceiver when the spatial wideband effect in time-domain or the corresponding beam squint effect in frequency-domain is taken into consideration. For this purpose, the frequency-domain mm-Wave channel matrix at the n^{th}sub-carrier is given as [41]

$$\boldsymbol{H}_{BQ}[n] = \gamma \sum_{i=1}^{N_{cl}} \sum_{l=1}^{N_{ray}} \alpha_{il} \boldsymbol{a}_r\left(\varphi_{i,l,n}\right) \boldsymbol{a}_t\left(\psi_{i,l,n}\right)^H e^{-j2\pi\tau_{i,l}f_n}, \tag{56}$$

where $\gamma = \sqrt{\frac{N_t N_r}{N_{cl} N_{ray}}}$ is the normalization factor, α_{il} is the complex gain of the l^{th} path in the i^{th} cluster, and $e^{-j2\pi\tau_{i,l}f_n}$ denotes the delay component, in which $\tau_{i,l}$ describes the delay corresponding to the l^{th} path in the i^{th} cluster. The frequency-dependent array response vectors $\boldsymbol{a}_t\left(\psi_{i,l,n}\right)$ and $\boldsymbol{a}_r\left(\varphi_{i,l,n}\right)$ at the transmitter and receiver, respectively, can be expressed as

$$\boldsymbol{a}_t\left(\psi_{i,l,n}\right) = \frac{1}{\sqrt{N_t}}\left[1,\ e^{j2\pi\psi_{i,l,n}}, \ldots, e^{j(N_t-1)2\pi\psi_{i,l,n}}\right]^T, \tag{57a}$$

$$\boldsymbol{a}_r\left(\varphi_{i,l,n}\right) = \frac{1}{\sqrt{N_r}}\left[1,\ e^{j2\pi\varphi_{i,l,n}}, \ldots, e^{j(N_r-1)2\pi\varphi_{i,l,n}}\right]^T, \tag{57b}$$

where $\psi_{i,l,n}$and $\varphi_{i,l,n}$indicate the respective spatial direction of the l^{th}path in the i^{th}cluster corresponding to the n^{th}sub-carrier. Moreover, $\psi_{i,l,n}$and $\varphi_{i,l,n}$can be obtained using the following relation as

$$\psi_{i,l,n} = \frac{f_n}{c} d \sin\left(\omega_{i,\,l}\right), \tag{58a}$$

$$\varphi_{i,l,n} = \frac{f_n}{c} d \sin\left(\mu_{i,\,l}\right), \tag{58b}$$

where $f_n = f_c + \frac{f_s}{N_{sub}}\left(n - 1 - \frac{N_{sub}-1}{2}\right)$, and f_c and $f_s$denote the central frequency and bandwidth, respectively, while $\omega_{i,\,l} \in [0,\ 2\pi)$and $\mu_{i,\,l} \in [0,\ 2\pi)$ are the AoD and AoA at the transmitter and receiver, respectively. In (58a) and (58b), $d = \frac{c}{2f_c} = \frac{\lambda}{2}$ specifies the antenna spacing and $\lambda$is the wavelength of signal at the central frequency.

The proposed algorithm maximizes array gain through RF beamforming components and minimizes interference among transmitted data streams via baseband processing matrices. This design strategy facilitates minimizing the impact of beam squint on the performance of the proposed hybrid precoding scheme. The number of antennas at communicating nodes and the number of data streams are set as $N_t = N_r = N_d = 16$ and $N_s = 4$, respectively. Moreover, two relay nodes, i.e., $K = 2$, are deployed between the source and destination to assist data transmission. It is worth highlighting that the number of RF chains is equal to the number of data streams while conducting computer simulations. The system parameters to generate simulations results

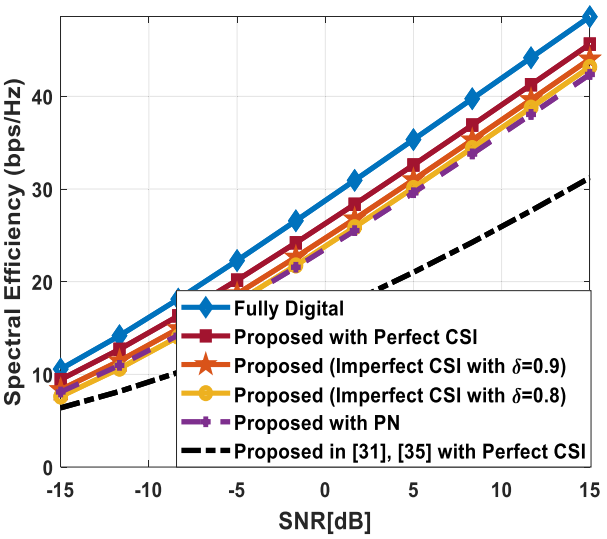

FIGURE 10. Spectral efficiency vs. SNR: Performance comparison between the proposed scheme and the hybrid precoding technique given in [31] and [35]. The number of antennas and transmitted data streams are set as $N_t = N_r = N_d = 16$ and $N_s = 8$.

TABLE 4. System parameters for simulation with beam squint.

Parameters	Values
Number of antennas at communicating nodes	$N_t = N_r = N_d = 16$
Number of data streams	$N_s = 4, 6$
Number of relay nodes	$K = 2, 4$
Number of sub-carriers	$N_{sub} = 128$
Number of RF chains	$N_t^{RF} = N_r^{RF} = N_d^{RF} = N_s$
Number of clusters,	$N_{cl} = 2, N_{ray} = 5$
Number of channel paths/cluster	
Central frequency	$f_c = 30\ GHz$
Bandwidth	$f_s = 3\ GHz$
Maximum time delay	$\tau_{max} = 20ns$

are summarized in Table 4, when the beam squint effect is taken into account. It is evident from the obtained results that the proposed hybrid precoding method achieves performance close to the upper bound defined by its full-complexity digital counterpart. Furthermore, the performance comparison of the proposed technique with other existing hybrid beamforming schemes is also shown in Fig. 12. The existing algorithms include alternating minimization (Alt-Min) based precoding [26], spatially sparse precoding [24], and hybrid wideband beamforming for beam squint compensation using space-time block coding (STBC) [51]. It is also obvious from Fig. 12 that the proposed method significantly outperforms these existing techniques.

Fig. 12 demonstrates the performance of the proposed scheme when four relay nodes (i.e., $K = 4$) are deployed between the source and destination for the transmission of

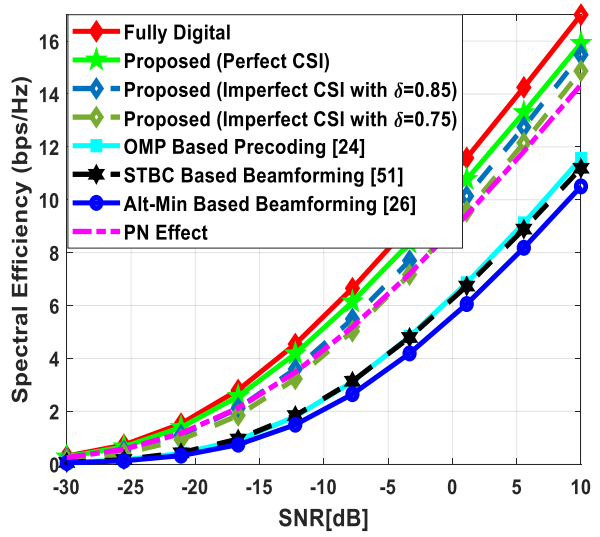

FIGURE 11. Spectral efficiency vs. SNR: Comparison between the proposed scheme and existing hybrid precoding algorithms, when $N_t = N_r = N_d = 16$, $N_s = 4$ and $K = 2$.

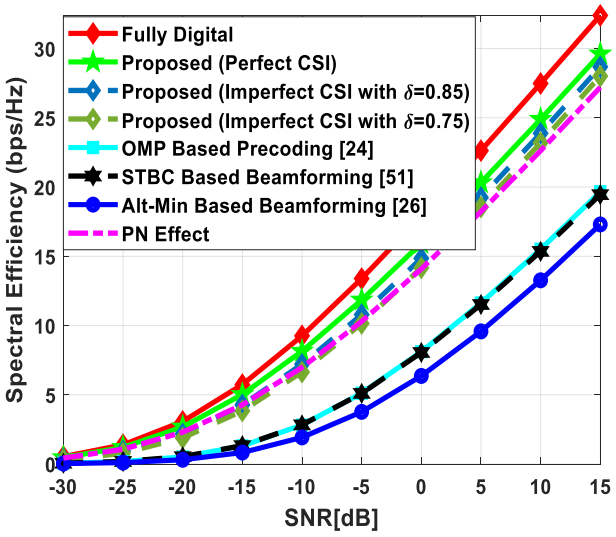

FIGURE 12. Spectral efficiency vs. SNR: Comparison between the proposed algorithm scheme and existing hybrid beamforming techniques, when $N_t = N_r = N_d = 16$, $N_s = 6$ and $K = 4$.

$N_s = 6$ data streams. The mm-Wave channel parameters and the number of antennas at communicating nodes are the same as in the previous case. It is clear from the obtained results that the proposed technique achieves performance close to that of unconstrained fully digital precoding, and the existing techniques suffer from similar performance degradation due to the beam-split effect, as seen in Fig. 12.

VII. CONCLUSION

This paper investigates the hybrid wideband beamforming design in a single-user multi-relay MIMO system for achievable rate maximization. The element-wise constant amplitude constraint associated with the analog beamforming component makes the problem non-convex and hence, mathematically intractable. Moreover, practical broadband systems require the RF processing solution common to all frequency sub-carriers, and this design challenge adds another layer of complexity in deriving the phase-only processing part of hybrid precoding under frequency-selective channels. For deriving the RF and baseband processing components that lead to achievable rate maximization, the original complicated optimization problem is transformed into a relatively simple form. Furthermore, an endeavor is made to decouple the design of analog RF and digital baseband processing components by exploiting the property of the unitary transform. Then, the problem of designing the analog beamforming solution is decomposed into sub-problems, and each sub-problem is tackled using the alternating minimization approach. In particular, the common analog precoder and combiner at the source and destination, respectively, are derived using the notion of tensor decomposition. To derive the phase-only precoder and combiner at each relay node, each sub-problem is transformed into L_1-norm maximization problem, as this objective function makes the design robust against channel imperfections and PN in hybrid beamformers. Finally, digital baseband processing components are obtained by minimizing interference among transmitted data streams through the sub-channels corresponding to the equivalent baseband channels. It is obvious from the obtained results that the proposed algorithm achieves acceptable performance by changing system parameters in the presence of channel estimation error and PN when compared with the theoretical upper bound. Moreover, the proposed scheme outperforms in comparison to the other existing hybrid beamforming methods. The extension of this work, considering intelligent reflecting surfaces, is a promising future direction.

APPENDIX A

Let $\sigma_1[n],\ \sigma_2[n], \ldots,\ \sigma_{n_{min}}[n]$ be the singular values of the effective channel $\boldsymbol{A}[n]$ from the source to the destination in (9) corresponding to the n^{th} frequency-carrier. Applying SVD on $\boldsymbol{A}[n]$ can decompose it into n_{min} independent parallel eigenchannels, where $\sigma_j[n]$ denotes the gain of the j^{th} channel. Hence, the capacity expression can be characterized as

$$C_n = \sum_{j=1}^{n_{min}} \log_2\left(1 + \frac{P_j[n]}{P_N}\sigma_j^2[n]\right)\left(\frac{pbs}{Hz}\right)$$

where $P_j[n] = \max\left(c - \frac{P_N}{\sigma_j^2[n]},\ 0\right)$ is the power allocated to the j^{th} channel according to the water filling algorithm and c denotes a constant satisfying the transmit power constraint $\sum_{j=1}^{n_{min}} P_j[n] = P_s, \forall n \in \{1, \ldots, N_{sub}\}$, and P_N indicates the noise power. Substituting $P_j[n]$ into the above-mentioned capacity formula leads to the following result:

$$C_n = \sum\nolimits_{P_j[n]\neq 0} \log_2\left(\frac{c}{P_N}\right) + \log_2\left(\Pi_{P_j[n]\neq 0}\sigma_j^2[n]\right)$$

where $\sigma_j^2[n]$ are the eigenvalues of $\boldsymbol{A}[n]\boldsymbol{A}^H[n]$. It is clear from the last expression that $\log_2\left(\Pi_{P_j[n]\neq 0}\sigma_j^2[n]\right)$ is highly dependent on $\boldsymbol{A}[n]$. Moreover, $\log_2\left(\Pi_{P_j[n]\neq 0}\sigma_j^2[n]\right)$ can also be expressed as $\sum_j \log_2\left(\sigma_j^2[n]\right)$. Therefore, the achievable rate maximization in (10) is simplified as $Tr\left\{\boldsymbol{A}[n]\boldsymbol{A}^H[n]\right\}$.

REFERENCES

[1] I. F. Akyildiz, A. Kak, and S. Nie, "6G and beyond: The future of wireless communications systems," *IEEE Access*, vol. 8, pp. 133995–134030, 2020, doi: 10.1109/ACCESS.2020.3010896.

[2] Z. Zhang, Y. Xiao, Z. Ma, M. Xiao, Z. Ding, X. Lei, G. K. Karagiannidis, and P. Fan, "6G wireless networks: Vision, requirements, architecture, and key technologies," *IEEE Veh. Technol. Mag.*, vol. 14, no. 3, pp. 28–41, Sep. 2019, doi: 10.1109/MVT.2019.2921208.

[3] K. Samdanis and T. Taleb, "The road beyond 5G: A vision and insight of the key technologies," *IEEE Netw.*, vol. 34, no. 2, pp. 135–141, Mar. 2020, doi: 10.1109/MNET.001.1900228.

[4] M. Giordani, M. Polese, M. Mezzavilla, S. Rangan, and M. Zorzi, "Toward 6G networks: Use cases and technologies," *IEEE Commun. Mag.*, vol. 58, no. 3, pp. 55–61, Mar. 2020, doi: 10.1109/MCOM.001.1900411.

[5] M. Z. Chowdhury, M. Shahjalal, S. Ahmed, and Y. M. Jang, "6G wireless communication systems: Applications, requirements, technologies, challenges, and research directions," *IEEE Open J. Commun. Soc.*, vol. 1, pp. 957–975, 2020, doi: 10.1109/OJCOMS.2020.3010270.

[6] J. Huang, C.-X. Wang, R. Feng, J. Sun, W. Zhang, and Y. Yang, "Multi-frequency mmWave massive MIMO channel measurements and characterization for 5G wireless communication systems," *IEEE J. Sel. Areas Commun.*, vol. 35, no. 7, pp. 1591–1605, Jul. 2017, doi: 10.1109/JSAC.2017.2699381.

[7] Q. Bi, "Ten trends in the cellular industry and an outlook on 6G," *IEEE Commun. Mag.*, vol. 57, no. 12, pp. 31–36, Dec. 2019, doi: 10.1109/MCOM.001.1900315.

[8] I. A. Hemadeh, K. Satyanarayana, M. El-Hajjar, and L. Hanzo, "Millimeter-wave communications: Physical channel models, design considerations, antenna constructions, and link-budget," *IEEE Commun. Surveys Tuts.*, vol. 20, no. 2, pp. 870–913, 2nd Quart., 2018, doi: 10.1109/COMST.2017.2783541.

[9] N. N. Moghadam, G. Fodor, M. Bengtsson, and D. J. Love, "On the energy efficiency of MIMO hybrid beamforming for millimeter-wave systems with nonlinear power amplifiers," *IEEE Trans. Wireless Commun.*, vol. 17, no. 11, pp. 7208–7221, Nov. 2018, doi: 10.1109/TWC.2018.2865786.

[10] C. Xing, X. Zhao, S. Wang, W. Xu, S. X. Ng, and S. Chen, "Hybrid transceiver optimization for multi-hop communications," *IEEE J. Sel. Areas Commun.*, vol. 38, no. 8, pp. 1880–1895, Aug. 2020, doi: 10.1109/JSAC.2020.3000808.

[11] C. Huang, Z. Yang, G. C. Alexandropoulos, K. Xiong, L. Wei, C. Yuen, Z. Zhang, and M. Debbah, "Multi-hop RIS-empowered terahertz communications: A DRL-based hybrid beamforming design," *IEEE J. Sel. Areas Commun.*, vol. 39, no. 6, pp. 1663–1677, Jun. 2021, doi: 10.1109/JSAC.2021.3071836.

[12] Q. Xia and J. M. Jornet, "Multi-hop relaying distribution strategies for terahertz-band communication networks: A cross-layer analysis," *IEEE Trans. Wireless Commun.*, vol. 21, no. 7, pp. 5075–5089, Jul. 2022, doi: 10.1109/TWC.2021.3136788.

[13] J. Du, Y. Zhang, Y. Chen, X. Li, Y. Cheng, and M. V. Rajesh, "Hybrid beamforming NOMA for mmWave half-duplex UAV relay-assisted B5G/6G IoT networks," *Comput. Commun.*, vol. 180, pp. 232–242, Dec. 2021.

[14] A. A. Nasir, H. D. Tuan, T. Q. Duong, H. V. Poor, and L. Hanzo, "Hybrid beamforming for multi-user millimeter-wave networks," *IEEE Trans. Veh. Technol.*, vol. 69, no. 3, pp. 2943–2956, Mar. 2020, doi: 10.1109/TVT.2020.2966122.

[15] M. Li, W. Liu, X. Tian, Z. Wang, and Q. Liu, "Iterative hybrid precoder and combiner design for mmWave MIMO-OFDM systems," *Wireless Netw.*, vol. 25, no. 8, pp. 4829–4837, Nov. 2019.

[16] L. Jiang and H. Jafarkhani, "Multi-user analog beamforming in millimeter wave MIMO systems based on path angle information," *IEEE Trans. Wireless Commun.*, vol. 18, no. 1, pp. 608–619, Jan. 2019, doi: 10.1109/TWC.2018.2883279.

[17] Z. Ding, P. Fan, and H. V. Poor, "Random beamforming in millimeter-wave NOMA networks," *IEEE Access*, vol. 5, pp. 7667–7681, 2017, doi: 10.1109/ACCESS.2017.2673248.

[18] A. A. Badrudeen, C. Y. Leow, and S. Won, "Performance analysis of hybrid beamforming precoders for multiuser millimeter wave NOMA systems," *IEEE Trans. Veh. Technol.*, vol. 69, no. 8, pp. 8739–8752, Aug. 2020, doi: 10.1109/TVT.2020.3000443.

[19] Y. Liu, Q. Feng, Q. Wu, Y. Zhang, M. Jin, and T. Qiu, "Energy-efficient hybrid precoding with low complexity for mmWave massive MIMO systems," *IEEE Access*, vol. 7, pp. 95021–95032, 2019, doi: 10.1109/ACCESS.2019.2928559.

[20] X. Gao, L. Dai, S. Han, and R. W. Heath, "Energy-efficient hybrid analog and digital precoding for mmWave MIMO systems with large antenna arrays," *IEEE J. Sel. Areas Commun.*, vol. 34, no. 4, pp. 998–1009, Apr. 2016, doi: 10.1109/JSAC.2016.2549418.

[21] S. He, C. Qi, Y. Wu, and Y. Huang, "Energy-efficient transceiver design for hybrid sub-array architecture MIMO systems," *IEEE Access*, vol. 4, pp. 9895–9905, 2016, doi: 10.1109/ACCESS.2017.2649539.

[22] X. Gao, L. Dai, Y. Sun, S. Han, and I. Chih-Lin, "Machine learning inspired energy-efficient hybrid precoding for mmWave massive MIMO systems," in *Proc. IEEE Int. Conf. Commun. (ICC)*, Paris, France, May 2017, pp. 1–6, doi: 10.1109/ICC.2017.7997065.

[23] Z. Wang, M. Li, H. Li, and Q. Liu, "Hybrid beamforming with one-bit quantized phase shifters in mmWave MIMO systems," in *Proc. IEEE Int. Conf. Commun. (ICC)*, Kansas City, MO, USA, May 2018, pp. 1–6, doi: 10.1109/ICC.2018.8422249.

[24] O. E. Ayach, S. Rajagopal, S. Abu-Surra, Z. Pi, and R. W. Heath, "Spatially sparse precoding in millimeter wave MIMO systems," *IEEE Trans. Wireless Commun.*, vol. 13, no. 3, pp. 1499–1513, Mar. 2014, doi: 10.1109/TWC.2014.011714.130846.

[25] F. Sohrabi and W. Yu, "Hybrid analog and digital beamforming for mmWave OFDM large-scale antenna arrays," *IEEE J. Sel. Areas Commun.*, vol. 35, no. 7, pp. 1432–1443, Jul. 2017, doi: 10.1109/JSAC.2017.2698958.

[26] X. Yu, J.-C. Shen, J. Zhang, and K. B. Letaief, "Alternating minimization algorithms for hybrid precoding in millimeter wave MIMO systems," *IEEE J. Sel. Topics Signal Process.*, vol. 10, no. 3, pp. 485–500, Apr. 2016, doi: 10.1109/JSTSP.2016.2523903.

[27] Z. Xiao, P. Xia, and X.-G. Xia, "Codebook design for millimeter-wave channel estimation with hybrid precoding structure," *IEEE Trans. Wireless Commun.*, vol. 16, no. 1, pp. 141–153, Jan. 2017, doi: 10.1109/TWC.2016.2619705.

[28] X. Zhai, Y. Cai, Q. Shi, M. Zhao, G. Y. Li, and B. Champagne, "Joint transceiver design with antenna selection for large-scale MU-MIMO mmWave systems," *IEEE J. Sel. Areas Commun.*, vol. 35, no. 9, pp. 2085–2096, Sep. 2017, doi: 10.1109/JSAC.2017.2720197.

[29] S. He, J. Wang, Y. Huang, B. Ottersten, and W. Hong, "Codebook-based hybrid precoding for millimeter wave multiuser systems," *IEEE Trans. Signal Process.*, vol. 65, no. 20, pp. 5289–5304, Oct. 2017, doi: 10.1109/TSP.2017.2723353.

[30] C. Lin, G. Y. Li, and L. Wang, "Subarray-based coordinated beamforming training for mmWave and sub-THz communications," *IEEE J. Sel. Areas Commun.*, vol. 35, no. 9, pp. 2115–2126, Sep. 2017, doi: 10.1109/JSAC.2017.2720038.

[31] J. Lee and Y. H. Lee, "AF relaying for millimeter wave communication systems with hybrid RF/baseband MIMO processing," in *Proc. IEEE Int. Conf. Commun. (ICC)*, Sydney, NSW, Australia, Jun. 2014, pp. 5838–5842, doi: 10.1109/ICC.2014.6884253.

[32] X. Xue, T. E. Bogale, X. Wang, Y. Wang, and B. L. Long, "Hybrid analog-digital beamforming for multiuser MIMO millimeter wave relay systems," in *Proc. IEEE/CIC Int. Conf. Commun. China (ICCC)*, Shenzhen, China, Nov. 2015, pp. 1–7, doi: 10.1109/ICCChina.2015.7448664.

[33] X. Xue, Y. Wang, L. Dai, and C. Masouros, "Relay hybrid precoding design in millimeter-wave massive MIMO systems," *IEEE Trans. Signal Process.*, vol. 66, no. 8, pp. 2011–2026, Apr. 2018, doi: 10.1109/TSP.2018.2799201.

[34] H. Abbas and K. Hamdi, "Millimeter wave communications over relay networks," in *Proc. IEEE Wireless Commun. Netw. Conf. (WCNC)*, San Francisco, CA, USA, Mar. 2017, pp. 1–6, doi: 10.1109/WCNC.2017.7925836.

[35] H. Abbas and K. Hamdi, "Hybrid beamformers design for MIMO relay networks in millimeter wave," in *Proc. IEEE Wireless Commun. Netw. Conf. (WCNC)*, San Francisco, CA, USA, Mar. 2017, pp. 1–6, doi: 10.1109/WCNC.2017.7925884.

[36] J.-S. Sheu, "Hybrid digital and analogue beamforming design for millimeter wave relaying systems," *J. Commun. Netw.*, vol. 19, no. 5, pp. 461–469, Oct. 2017, doi: 10.1109/JCN.2017.000078.
[37] C. G. Tsinos, S. Chatzinotas, and B. Ottersten, "Hybrid analog-digital transceiver designs for mmWave amplify-and-forward relaying systems," in *Proc. 41st Int. Conf. Telecommun. Signal Process. (TSP)*, Athens, Greece, Jul. 2018, pp. 1–6, doi: 10.1109/TSP.2018.8441203.
[38] Y. Chen, D. Chen, Y. Tian, and T. Jiang, "Spatial lobes division-based low complexity hybrid precoding and diversity combining for mmWave IoT systems," *IEEE Internet Things J.*, vol. 6, no. 2, pp. 3228–3239, Apr. 2019, doi: 10.1109/JIOT.2018.2881171.
[39] Y. Chen, D. Chen, and T. Jiang, "Non-uniform quantization codebook-based hybrid precoding to reduce feedback overhead in millimeter wave MIMO systems," *IEEE Trans. Commun.*, vol. 67, no. 4, pp. 2779–2791, Apr. 2019, doi: 10.1109/TCOMM.2018.2890227.
[40] Y. Chen, D. Chen, T. Jiang, and L. Hanzo, "Channel-covariance and angle-of-departure aided hybrid precoding for wideband multiuser millimeter wave MIMO systems," *IEEE Trans. Commun.*, vol. 67, no. 12, pp. 8315–8328, Dec. 2019, doi: 10.1109/TCOMM.2019.2942307.
[41] Y. Chen, Y. Xiong, D. Chen, T. Jiang, S. X. Ng, and L. Hanzo, "Hybrid precoding for WideBand millimeter wave MIMO systems in the face of beam squint," *IEEE Trans. Wireless Commun.*, vol. 20, no. 3, pp. 1847–1860, Mar. 2021, doi: 10.1109/TWC.2020.3036945.
[42] G. M. Zilli and W.-P. Zhu, "Constrained tensor decomposition-based hybrid beamforming for mmWave massive MIMO-OFDM communication systems," *IEEE Trans. Veh. Technol.*, vol. 70, no. 6, pp. 5775–5788, Jun. 2021, doi: 10.1109/TVT.2021.3076691.
[43] M. Ruble and I. Güvenç, "Multilinear singular value decomposition for millimeter wave channel parameter estimation," *IEEE Access*, vol. 8, pp. 75592–75606, 2020, doi: 10.1109/ACCESS.2020.2988485.
[44] A. F. Molisch, V. V. Ratnam, S. Han, Z. Li, S. L. H. Nguyen, L. Li, and K. Haneda, "Hybrid beamforming for massive MIMO: A survey," *IEEE Commun. Mag.*, vol. 55, no. 9, pp. 134–141, Sep. 2017, doi: 10.1109/MCOM.2017.1600400.
[45] F. Rusek, D. Persson, B. K. Lau, E. G. Larsson, T. L. Marzetta, O. Edfors, and F. Tufvesson, "Scaling up MIMO: Opportunities and challenges with very large arrays," *IEEE Signal Process. Mag.*, vol. 30, no. 1, pp. 40–60, Jan. 2013, doi: 10.1109/MSP.2011.2178495.
[46] M. M. Molu, P. Xiao, M. Khalily, K. Cumanan, L. Zhang, and R. Tafazolli, "Low-complexity and robust hybrid beamforming design for multi-antenna communication systems," *IEEE Trans. Wireless Commun.*, vol. 17, no. 3, pp. 1445–1459, Mar. 2018, doi: 10.1109/TWC.2017.2778258.
[47] L. Jiang and H. Jafarkhani, "MmWave amplify-and-forward MIMO relay networks with hybrid precoding/combining design," *IEEE Trans. Wireless Commun.*, vol. 19, no. 2, pp. 1333–1346, Feb. 2020, doi: 10.1109/TWC.2019.2953032.
[48] W. Ni and X. Dong, "Hybrid block diagonalization for massive multiuser MIMO systems," *IEEE Trans. Commun.*, vol. 64, no. 1, pp. 201–211, Jan. 2016, doi: 10.1109/TCOMM.2015.2502954.
[49] T.-H. Tsai, M.-C. Chiu, and C.-C. Chao, "Sub-system SVD hybrid beamforming design for millimeter wave multi-carrier systems," *IEEE Trans. Wireless Commun.*, vol. 18, no. 1, pp. 518–531, Jan. 2019, doi: 10.1109/TWC.2018.2882490.
[50] J. M. Hamamreh, E. Basar, and H. Arslan, "OFDM-subcarrier index selection for enhancing security and reliability of 5G URLLC services," *IEEE Access*, vol. 5, pp. 25863–25875, 2017, doi: 10.1109/ACCESS.2017.2768558.
[51] X. Liu and D. Qiao, "Space-time block coding-based beamforming for beam squint compensation," *IEEE Wireless Commun. Lett.*, vol. 8, no. 1, pp. 241–244, Feb. 2019.

HAFIZ MUHAMMAD TAHIR MUSTAFA received the B.Sc. degree in electrical engineering from the University of Engineering and Technology (UET) Lahore, Pakistan, the M.S. degree in signal processing and machine intelligence from the University of Surrey, U.K., in 2010, and the Ph.D. degree in electrical engineering from Kangwon National University (KNU), Republic of Korea, in 2022. His research interests include mobile wireless communication, signal processing, machine learning, deep learning, and image processing.

JUNG-IN BAIK was born in Seoul, South Korea, in 1984. He received the B.S. and Ph.D. degrees in information and communication engineering from Sejong University, South Korea, in 2007 and 2013, respectively. Since 2021, he has been a Research Professor with the Department of Information and Communication Engineering, Sejong University. His research interests include cooperative MIMO communication, beamforming, intelligent reflecting surface (IRS), and deep learning.

YOUNG-HWAN YOU received the B.S., M.S., and Ph.D. degrees in electronic engineering from Yonsei University, Seoul, South Korea, in 1993, 1995, and 1999, respectively. From 1999 to 2002, he was a Senior Researcher with the Wireless PAN Technology Project Office, Korea Electronics Technology Institute (KETI), South Korea. Since 2002, he has been a Professor with the Department of Computer Engineering, Sejong University, Seoul. His research interests include wireless communications systems design, spread spectrum transceivers, and system architecture for realizing advanced digital communications systems, especially, for wireless OFDM.

ZUNIRA ABBASI received the B.E. degree in electronic engineering from Iqra University, Karachi, Pakistan, in 2017. She is currently pursuing the M.S. degree with the Department of Information and Communication Engineering, Sejong University, Republic of Korea. Her research interests include relay-based hybrid beamforming, machine learning, wireless communication, intelligent reflective surfaces, and the IoT applications.

HYOUNG-KYU SONG received the B.S., M.S., and Ph.D. degrees in electronic engineering from Yonsei University, Seoul, South Korea, in 1990, 1992, and 1996, respectively. From 1996 to 2000, he was a Managerial Engineer with the Korea Electronics Technology Institute (KETI), South Korea. Since 2000, he has been a Professor with the Department of Information and Communication Engineering and the Department of Convergence Engineering for Intelligent Drone, Sejong University, Seoul. His research interests include digital and data communications, information theory, and their applications with an emphasis on mobile communications.